NEUROSCIENCE

Functional imaging and quantification of multineuronal olfactory responses in *C. elegans*

Albert Lin[1,2]*†, Shanshan Qin[2,3], Helena Casademunt[1,2], Min Wu[4], Wesley Hung[4], Gregory Cain[1], Nicolas Z. Tan[5], Raymond Valenzuela[5], Leila Lesanpezeshki[4], Vivek Venkatachalam[5], Cengiz Pehlevan[2,3]*, Mei Zhen[4]*, Aravinthan D.T. Samuel[1,2]*

Many animals perceive odorant molecules by collecting information from ensembles of olfactory neurons, where each neuron uses receptors that are tuned to recognize certain odorant molecules with different binding affinity. Olfactory systems are able, in principle, to detect and discriminate diverse odorants using combinatorial coding strategies. We have combined microfluidics and multineuronal imaging to study the ensemble-level olfactory representations at the sensory periphery of the nematode *Caenorhabditis elegans*. The collective activity of *C. elegans* chemosensory neurons reveals high-dimensional representations of olfactory information across a broad space of odorant molecules. We reveal diverse tuning properties and dose-response curves across chemosensory neurons and across odorants. We describe the unique contribution of each sensory neuron to an ensemble-level code for volatile odorants. We show that a natural stimuli, a set of nematode pheromones, are also encoded by the sensory ensemble. The integrated activity of the *C. elegans* chemosensory neurons contains sufficient information to robustly encode the intensity and identity of diverse chemical stimuli.

INTRODUCTION

Many animals exhibit diverse behaviors—navigating the world, finding food, avoiding dangers—in response to olfactory cues. To do this, their olfactory systems distinguish the identity and intensity of numerous odorant molecules.

Insect and mammalian olfactory systems use large ensembles of olfactory sensory neurons to detect odorants and pheromones (*1*–*6*). Each olfactory sensory neuron usually expresses a specific olfactory receptor tuned to recognize odorant molecules by ligand-receptor binding affinity (*7*). A given receptor is typically activated by many different odorant molecules, and each odorant can activate multiple receptors (*1*, *8*). These olfactory systems can potentially use combinatorial coding strategies to distinguish and identify large numbers of odorant molecules.

Caenorhabditis elegans senses many odorants across wide concentration ranges (*9*–*11*). However, its olfactory circuits have a compact cellular and molecular organization that differs from insects and mammals (Fig. 1A). The *C. elegans* genome encodes >1000 putative chemosensory G protein–coupled receptors (GPCRs) (*12*, *13*); at least 200 GPCRs are expressed by its 11 pairs of amphid chemosensory neurons. This suggests both a substantial capacity for olfactory detection and a coding strategy where the properties of each neuron are shaped by many receptors (*12*–*14*).

C. elegans chemosensory neurons have been characterized as individual sensors for specific modalities from volatile odorants (AWA, AWB, and AWC) (*15*–*21*), soluble chemicals (ASE) (*22*, *23*), and ascaroside pheromones (ADL, ASK, and ADF) (*24*–*29*) to nociception (ASH) (*10*, *30*–*33*). A few chemosensory neurons detect gases (CO_2 and O_2) or temperature changes, in addition to odorants (*12*, *34*).

Behavioral studies first established AWA, AWB, and AWC to be the primary detectors of odorants. Laser ablation of AWA or AWC severely degrades chemotaxis toward selected attractive odorants. However, when both AWA and AWC are ablated, animals could move toward odorant sources (*35*). In similar experiments with selected organic compounds and salts, ablation of other chemosensory neurons—ASE, ADF, ASG, ASI, ASJ, and ASK—degrades chemotaxis to a lesser extent (*10*). Therefore, although some neurons are more important for chemotaxis toward some odorants than others, chemosensation does not rely on single neurons.

The stimulus-evoked properties of *C. elegans* chemosensory neurons have also been described through the detection of selected odorants by selected neurons (*15*–*21*). For example, isoamyl alcohol is detected by AWC, AWB, and ASH (*15*), and benzaldehyde is detected by AWA, AWB, AWC, and ASE (*17*). AWA responds to a wide range of volatile odorants (*16*). Diacetyl is detected by AWA at low concentrations and by ASH at high concentrations, as well as by AWC, ASK, and ASE. In some cases, the left and right pairs of a chemosensory neuron type detect different odorant molecules. For example, the left and right AWC neurons, AWCL and AWCR, are stochastically asymmetric, where one detects butanone and the other detects 2,3-pentanedione (*36*, *37*). The ASE neurons, primarily gustatory, respond asymmetrically to different ions, where ASEL detects sodium ions and ASER detects chloride and potassium ions (*22*, *23*).

We know less about the response properties of odorant receptors. ODR-10 remains its most thoroughly characterized odorant receptor, expressed in AWA and sensitive to diacetyl, an attractive stimulus. Ectopic expression of ODR-10 in AWB leads to diacetyl repulsion. This suggests that the attractive and aversive behaviors are encoded by the neuron, instead of specific odorants (*38*). Consistently, AWB and AWC are also needed for aversive olfactory

[1]Department of Physics, Harvard University, Cambridge, MA, USA. [2]Center for Brain Science, Harvard University, Cambridge, MA, USA. [3]John A. Paulson School of Engineering and Applied Sciences, Harvard University, Cambridge, MA, USA. [4]Lunenfeld-Tanenbaum Research Institute, Mount Sinai Hospital, Toronto, ON, Canada. [5]Department of Physics, Northeastern University, Boston, MA, USA.
*Corresponding author. Email: albertlin@g.harvard.edu (A.L.); cpehlevan@seas.harvard.edu (C.P.); meizhen@lunenfeld.ca (M.Z.); samuel@g.harvard.edu (A.D.T.S.)
†Present address: Princeton Neuroscience Institute and The Center for the Physics of Biological Function, Princeton University, Princeton, NJ, USA.

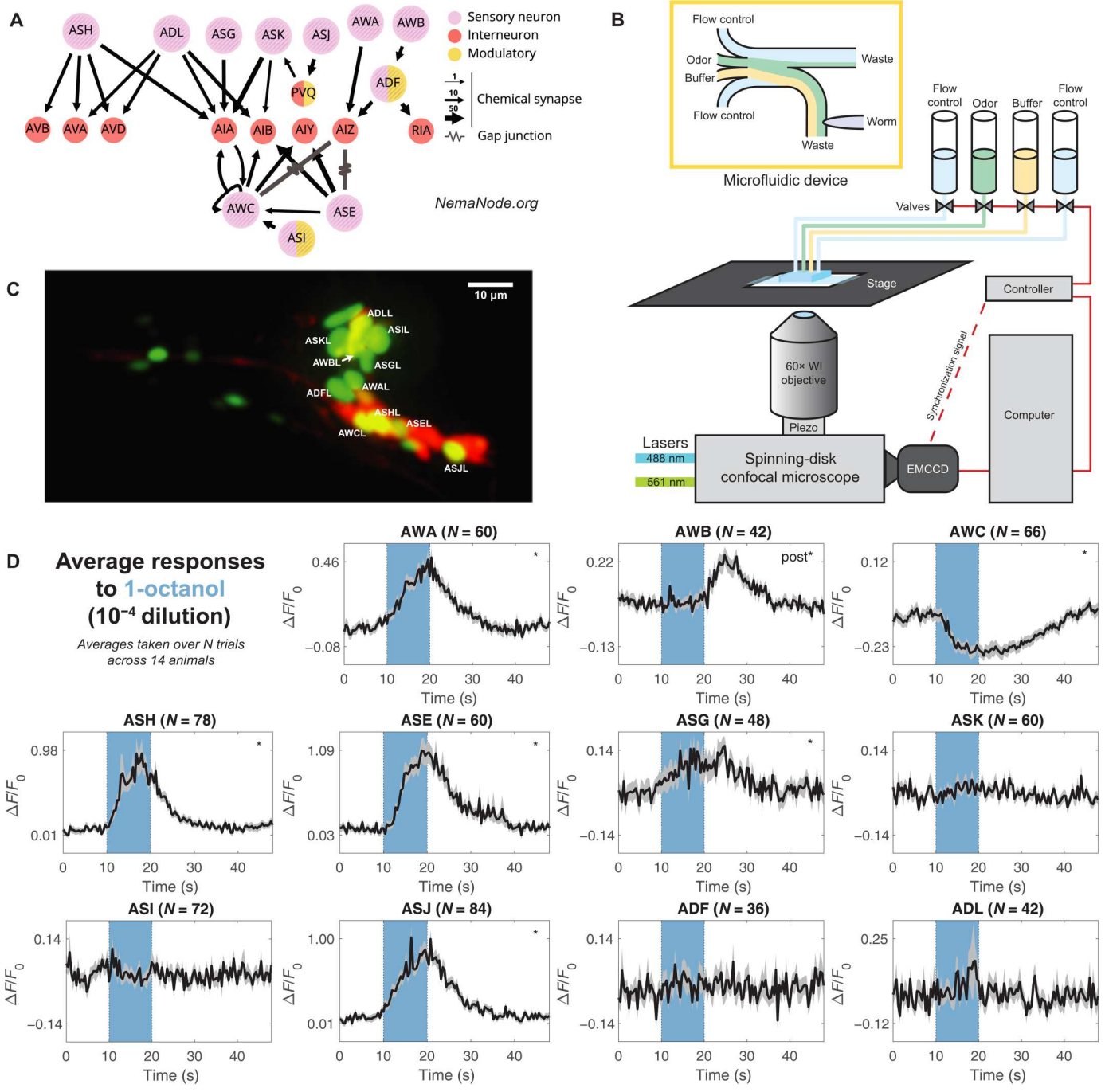

Fig. 1. Labeling and recording from chemosensory neurons. (**A**) Downstream partners of the 11 chemosensory neurons in the *C. elegans* connectome (*55*, *56*). Panel generated at nemanode.org. (**B**) Adult *C. elegans* were immobilized inside a microfluidic device and controllably presented with odorant solutions. Each animal was volumetrically imaged at 2.5 Hz with a spinning-disk confocal microscope during stimulus presentations. EMCCD, electron multiplying charge-coupled device; WI, water-immersion. (**C**) Animals expressed nuclear-localized GCaMP6s in all ciliated sensory neurons. A sparse wCherry landmark distinguished the 11 chemosensory neurons. Here, a dual-color maximum projection image shows the head of the worm. The 11 chemosensory neurons on the near (L) side are labeled. For clarity, the chemosensory neurons on the far side and other ciliated neurons are not labeled. (**D**) Neuronal activity traces of the 11 chemosensory neurons in response to a single odorant presentation (1-octanol, 10^{-4} dilution), averaged across multiple trials across 14 animals. The number of trials varies across neurons because neurons that were occluded or improperly tracked were excluded from the dataset (see Materials and Methods). The 10-s odorant delivery period is shown by the colored bar. Significant responses ($q \leq 0.01$) are marked with stars, with "post" indicating a significant response to stimulus removal (OFF response). Error bars (gray) are SEM.

learning (*39*, *40*) and activating different subsets of chemosensory neurons changes the activity of different downstream interneurons (*41*).

Complex properties of individual neurons and their relationships to behaviors have been extensively examined. AWC, ASH, and ASE exhibit adaptation: When a chemical stimulus is prolonged from minutes to hours, both neuronal activity and behavioral responses diminish (*16*, *42*–*45*). AWA and AWC change their response properties in a context-dependent manner (*46*, *47*). AWA neurons fire action potentials that may encode stimulus-specific features (*48*). Complex activity patterns of AWA have been directly mapped to behavioral patterns (*16*, *17*, *38*, *48*, *49*).

Although odorant-evoked responses in many individual *C. elegans* chemosensory neurons are well characterized, how their collective dynamics might represent odorant information as an ensemble remains unexamined. We set out to characterize how this chemosensory ensemble responds to a chemically diverse space of odorants at different concentrations and how the tuning properties of each chemosensory neuron might relate to an ensemble-level code. We assembled a panel of olfactory stimuli spanning a diverse molecular chemistry and used microfluidics to deliver these odorants at multiple concentrations (Fig. 1B). To efficiently record neuronal responses at the sensory periphery, we used a transgenic animal that allowed simultaneous measurement of intracellular calcium dynamics in all amphid chemosensory neurons (Fig. 1, A and C).

We found that most odorant-evoked responses are widespread across the chemosensory ensemble. Dose-response curves are different for different odorant molecules, whether comparing the responses of the same neuron to different odorants or comparing the responses of different neurons to the same odorant. Odorant identity and intensity information can be reliably decoded by the collective activity of the chemosensory ensemble. A set of pheromones also evokes ensemble-level responses but with a distinct pattern from volatile odorants. We conclude that the ensemble-level representations of different odorants in the small sensory system of *C. elegans* contain sufficient information to accurately distinguish the identity and intensity of odorant molecules across olfactory stimulus space.

RESULTS

Calcium imaging of chemosensory neurons with representative odorant stimuli

We developed a GCaMP6s calcium reporter line to simultaneously record calcium dynamics in all ciliated sensory neurons (Supplementary Methods and fig. S1). We focused on the 11 pairs of amphid chemosensory neurons: AWA, AWB, AWC, ASE, ASG, ASH, ASI, ASJ, ASK, ADL, and ADF (Fig. 1A). We immobilized and positioned young adult *C. elegans* in a microfluidic device that allows odorants to flow past its nose (Fig. 1B) (*50*). We adapted a multichannel microfluidic device (*4*) to control the delivery of pulses of single and mixed odorant solutions. Volumetric imaging was performed at 2.5 Hz with a spinning-disk confocal microscope (Fig. 1, B to D, and fig. S2).

We assembled a stimulus panel of 23 odorants, selected to span the chemical diversity of 122 previously studied molecules in *C. elegans* olfaction (*35*, *51*). We included exemplars of six chemical classes: alcohols (1-pentanol, 1-hexanol, 1-heptanol, 1-octanol, 1-nonanol, isoamyl alcohol, and geraniol), aromatics (benzaldehyde and methyl salicylate), esters (ethyl acetate, ethyl butyrate, pentyl acetate, ethyl heptanoate, and butyl butyrate), ketones (2-butanone, diacetyl, 2-heptanone, 2-nonanone, and 2,3-pentanedione), pyrazines (2,5-dimethyl pyrazine and 2-methyl pyrazine), and thiazoles (2-isobutylthiazole and 2,4,5-trimethylthiazole). To assess chemical diversity, we constructed a geometrical odor space using physical and chemical descriptors of molecular structure (*52*). Our 23 odorants broadly sample this geometrical space (fig. S3, A and B) (*52*).

We recorded the responses of all amphid chemosensory neurons to >70 stimulus conditions, testing each of the 23 odorants at multiple concentrations. Individual animals were repeatedly presented with series of 10-s odorant pulses separated by 30-s buffer blanks (fig. S2, A and B). For each stimulus condition, we recorded the responses to ~80 odor presentations across multiple animals (Fig. 2, A to C, and fig. S3, C and D). The highest concentrations we tested were 10^{-4} dilutions. The lowest concentrations we tested (10^{-8} dilutions) did not elicit significant responses from any neuron.

Odorants elicit ensemble responses

Across our odorant panel, calcium imaging captured many sensory neuron responses, some previously characterized and some unknown. Nearly every odorant reliably activated more sensory neurons than previously described. For example, diacetyl, attractive at low concentrations (*53*), reliably activated AWA upon odor onset at all concentrations (Fig. 2, A to C). 1-Octanol, a repellent (*54*), reliably activated ASH and inhibited AWC across concentrations (Fig. 2, A to C). However, additional reliable responses were also uncovered. For example, AWC was inhibited by butyl butyrate, and ASJ was activated by 1-octanol. Similarly, isoamyl alcohol not only activated AWA, AWB, AWC, and ASH at different concentrations, as previously reported (*15*), but also activated ASE and ASG (Fig. 2, A to C). At high concentrations, every odorant elicited responses from multiple sensory neurons. We observed substantial overlap in the sets of responding neurons for different odorants (Fig. 2, A to D).

Most chemosensory neurons exhibited ON responses to most odorants—changes in calcium levels upon odorant onset. We also observed OFF responses—changes in calcium levels upon odorant removal. For example, AWB has been reported to exhibit ON and OFF responses at different isoamyl alcohol concentrations (*15*). We confirmed this result and also found that AWB had ON responses to some odorants, such as diacetyl at high concentration, and OFF responses to 1-hexanol and 1-octanol (Fig. 1D and fig. S2E).

Most chemosensory neurons exhibited excitatory responses—increases in intracellular calcium levels during stimulus presentation. Some neurons exhibited inhibitory responses—decreases in intracellular calcium levels below the baseline level. A previous work showed that AWC is inhibited by several odorants in our panel, including diacetyl, benzaldehyde, and 2-butanone (*16*, *17*, *21*, *39*). In our stimulus conditions, AWC is inhibited by every odorant in our panel (Fig. 2A). We also found that ASK is inhibited by many odorants including ethyl butyrate and 2-nonanone (fig. S2F). Some neurons are inhibited by certain odorants but excited by others. For example, ASJ is strongly inhibited by 2-butanone but strongly excited by 1-nonanol (fig. S2G).

The left and right ASE neurons exhibited strong asymmetry in their responses to two odorants—heptanoate and butyl butyrate. Both activated ASEL and inactivated ASER (fig. S2H). AWC,

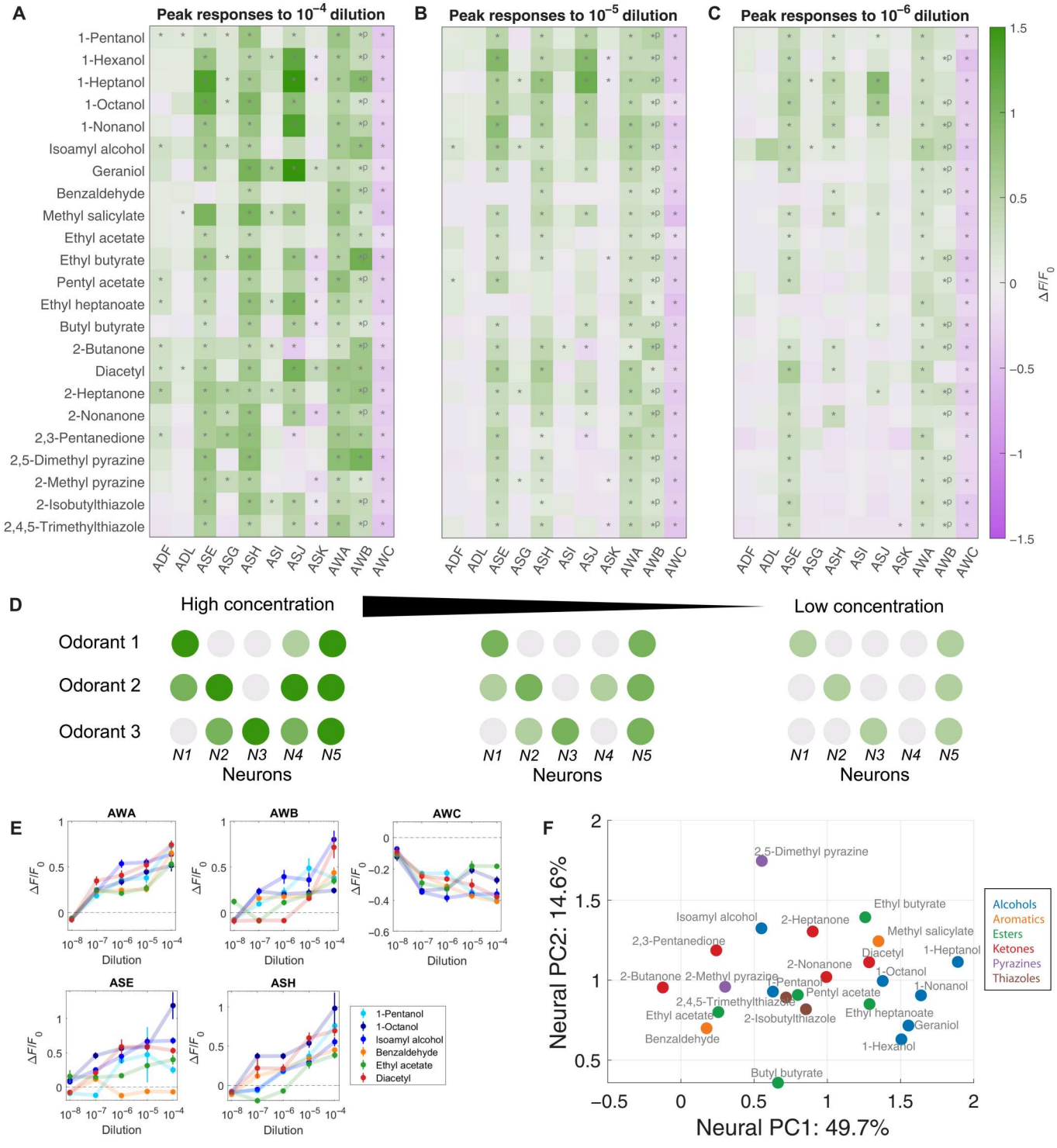

Fig. 2. Ensemble responses to a broad odorant panel. Average peak responses of the 11 chemosensory neurons to odorants at (**A**) high concentration (10^{-4} dilution), (**B**) medium concentration (10^{-5} dilution), and (**C**) low concentration (10^{-6} dilution). Peaks were computed from a time window from onset of odor delivery to 10 s after odor removal. Responses are reported as $\Delta F/F_0$. Significant responses ($q \leq 0.01$, two-tailed, paired *t* tests) are indicated with stars. Significant OFF responses are indicated with *P. Most odorants elicit significant responses from unique neuron combinations. (**D**) Schematic of coding strategy observed in (A) to (C). Different odorants evoke responses in distinct subsets of sensory neurons. Responses are generally stronger at high concentrations. Additional neurons are activated as concentration increases. (**E**) Dose responses of the peak responses of AWA, AWB, AWC, ASE, and ASH are diverse, with distinct concentration-dependent curves in response to different odorants. See fig. S3F for dose responses of the other six sensory neurons. Error bars are SEM. (**F**) PC space built from standardized peak average neural responses. Chemical class is indicated by color. Some odorant classes, such as alcohols and ketones, have more similar neural representations, while other odorant classes, such as esters, have more diverse representations. See fig. S3I for PC loadings.

another pair of neurons with known structural asymmetry (*20*), might exhibit moderate differences in their response dynamics when presented with short odorant pulses (*21*). Because all other left and right sensory neurons respond symmetrically to all odorants and because the left and right ASE and AWC neurons also respond symmetrically to many odorants, we grouped left and right sensory neurons in all analyses unless otherwise noted.

To compare the temporal dynamics of chemosensory neurons across odorants, we computed pairwise cross-correlations of their activity time courses across odorants (fig. S4, A and B). We found that matrices of pairwise cross-correlations are distinct for different odorants. Measured in terms of peak responses or dynamics, the diversity of ensemble-level dynamics is as large as the number of tested odorants. The compact sensory neuron ensemble of *C. elegans* may be able to encode the identities of numerous odorants by using this combinatorially large space of distinct activity patterns.

Sensory representations are not dependent on chemical synaptic connections

The *C. elegans* connectomes have revealed consistent axo-axonic chemical synapses between some sensory neurons and from some interneurons to sensory neurons (Fig. 1A) (*55*, *56*). These connections raise the possibility that ensemble representations might not solely reflect independent responses from individual neurons.

We examined this possibility by analyzing ensemble responses in an *unc-13(s69)* mutant where synaptic vesicle fusion is mostly blocked (*57*) (Fig. 3A). We sampled five odorants that represent different chemical classes. In all cases, nearly identical groups of neurons significantly responded ($q \leq 0.01$) in wild-type and *unc-13* mutants (Fig. 3B). Therefore, chemical synaptic transmission does not appear to be the dominant factor in ensemble responses. The tuning of each neuron to an odorant is likely to be cell intrinsic, a function of the receptors expressed in each neuron.

It is possible that gap junctions or neuromodulation, which are not affected in *unc-13* mutants, play roles in shaping sensory responses. We note that there are no direct gap junctions between different chemosensory neurons (Fig. 1A). We also note that response magnitudes in *unc-13* mutants, on average across neurons and stimuli, were ~60% the size of response magnitudes in wild-type animals. Chemical synaptic connections might play a role in amplifying response magnitudes.

Olfactory representations broaden with increasing concentrations

We compared the response properties of different neurons in response to odorants from our panel over three to five orders of magnitude in concentration (Fig. 2, A to C, and fig. S3, C and D). For most odorants and neurons, response magnitudes increased monotonically with odorant concentration—neurons activated at low concentrations were also activated at all higher concentrations. Every odorant is associated with the activation of a characteristic set of neurons at all concentrations above detection threshold. Across all concentrations, for example, 1-pentanol activates AWA and AWC; 1-octanol activates ASE, ASH, AWA, AWB, and AWC; and benzaldehyde activates AWA, AWB, and AWC. Each set of activated neurons may constitute a unique olfactory representation associated with each odorant identity.

For many odorants, increasing concentration spatially broadens olfactory representation by activating more sensory neurons. Different neurons exhibit different thresholds for different odorants. For example, AWB is only activated by 1-pentanol at concentrations above 10^{-5} dilution, and ADF, ADL, and ASG are only significantly activated by 1-pentanol at 10^{-4} dilution, the highest tested concentration (fig. S3E). Thus, odorant intensity is represented partly by the magnitude of responses of activated neurons and partly by the number and identities of activated neurons (Fig. 2D).

We used phase-trajectory analysis to illustrate the temporal dynamics of ensemble-level odorant representations. In a low-dimensional principal component (PC) space, these representations follow closed trajectories as they evolve over time following odor presentation (fig. S4C). Along each trajectory, neurons become activated, reach their peak responses, and return to baseline. In this space, the responses to different odorants follow trajectories with different headings from the origin. Trajectories for responses to the same odorant at different concentrations are aligned in direction but differ in magnitude.

Diversity in dose responses across neurons and odorants

We constructed dose-response curves for all 11 chemosensory neurons in response to select odorants from our panel over five orders of magnitude in concentration. The dose-response curves of the 11 chemosensory neurons exhibit substantial diversity (Fig. 2E and fig. S3F). Each odorant can evoke dose-response curves with different thresholds and steepnesses in different neurons. Conversely, each sensory neuron can exhibit dose-response curves with different thresholds and steepnesses for different odorants.

In some cases, neurons detected an odorant with slowly graded responses over a broad dynamic range. Graded responses include AWA's response to 1-pentanol and ASG's response to 1-octanol (Fig. 2E and fig. S3F). In other cases, neurons exhibited steep response functions, becoming fully activated or fully inhibited above a sharply defined threshold. Step-like responses include ASE's response to 1-pentanol and AWB's response to 1-octanol.

To estimate differences in response steepness across odorants and neurons, we performed log-linear fits on peak responses r as a function of odorant dilution c: $r(c) \approx m\log_{10}c + I$ and determined the slope m through linear regression. Response steepnesses were diverse, whether for a given neuron across odorants or for a given odorant across neurons (fig. S3G).

Diversity in dose-response curves contrasts with insects and mammals, where olfactory sensory neurons exhibit similarly shaped dose-response curves across neurons and across odorants (*4*, *58*, *59*). In insects and mammals, each sensory neuron is generally equipped with one receptor type, whereas in *C. elegans*, each neuron likely expresses multiple receptors (*12*, *13*). For a nematode neuron, the presence of receptors to multiple odorants, each with different binding affinities, may explain dose-response diversity.

Comparing ensemble-level representations of chemically similar odorants

Different odorants activate distinct but overlapping subsets of the chemosensory ensemble (Fig. 2, A to C). Quantitative differences in the sensitivity of chemosensory neurons to odorants will depend on cell-specific patterns of receptor expression. In most olfactory systems, a typical olfactory receptor is activated by a range of

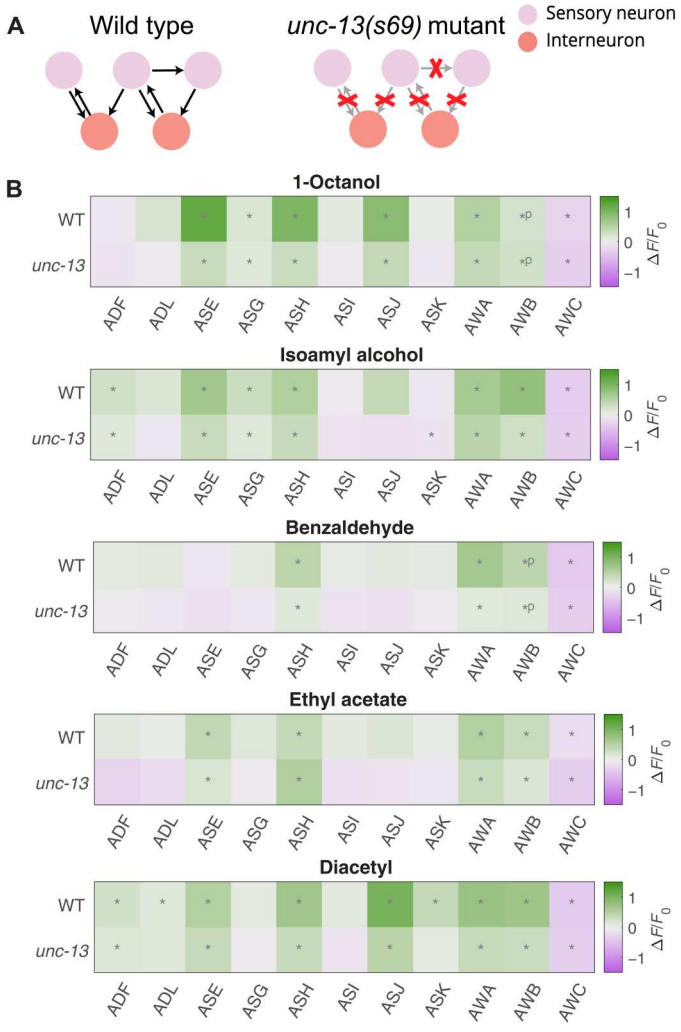

Fig. 3. Odorant representations in synaptic transmission mutants. (**A**) Most of the chemical synapses in *unc-13(s69)* synaptic transmission mutants are nonfunctional. We recorded neural activity in these mutants during odor presentation. (**B**) When presented with the same odorants, similar sets of neurons significantly ($q \leq 0.01$) responded in wild-type (WT) and *unc-13* mutants. Significant OFF responses are indicated with *P.

structurally similar odorant molecules with common chemical features. This leads to a systematic dependence of ensemble-level olfactory representations on odorant chemistry. To assess this dependence in *C. elegans*, we performed hierarchical clustering of odorants from our panel based on ensemble-level responses evoked at high concentrations (fig. S3H). The representations of some molecular classes clustered together. For example, ensemble-level responses to a set of straight-chain alcohols (1-hexanol, 1-heptanol, 1-octanol, and 1-nonanol) were similar to one another, and the ensemble-level responses to a set of ketones (2-butanone, 2,3-pentanedione, and 2-heptanone) were likewise similar. On the other hand, the esters in our panel, a group more diverse in their chemical structure, produced a broader set of representations.

Principal components analysis (PCA) is a quantitative means of comparing high-dimensional ensemble-level representations. We constructed a PC space from all average ensemble-level peak responses. We found that the first two PCs contain 65% of the variance (fig. S3I). The loading of the first two PCs allows us to assess the relative contribution of each sensory neuron to ensemble representations (fig. S3I). We observed a broad distribution of PC loading, which indicates a distributed contribution from all neurons to the separability of odorant representations.

We then asked how different odorants are distributed in the reduced PC space. Overall, the PC space appears compact without distinct clusters (Fig. 2F). Consistent with observations from hierarchical clustering, responses to certain classes of odorants, such as the straight-chain alcohols and two thiazoles, are close to each other in PC space. Responses to members of other classes, such as esters, are distributed more broadly.

Sensory neurons are either broadly or narrowly tuned in the chemical space

Olfactory sensory neurons are tuned to odorants by the relative binding affinities of receptors for different ligands (*7*). In animals where sensory neurons express single-receptor types, this leads to a systematic dependence of ensemble representation on the chemical properties of odorants and receptors (*4*, *7*, *60*, *61*). In *C. elegans*, the tuning of a sensory neuron may also be shaped by the expression of multiple different receptors. To explore the tuning of sensory neurons in chemical space, we projected the activity of each neuron into a PC space based on the chemical structure of odorants (fig. S3A) (*52*).

We observed a qualitative distinction in neuron tuning. Neurons AWA, AWB, AWC, and ASE each respond to most tested odorants at high concentrations, so we call them "broadly tuned" (Figs. 2, A to C, and 4A). In contrast, ADF, ADL, ASG, ASI, ASJ, and ASK each respond to a smaller set of odorants even at the highest tested concentrations, so we call them "narrowly tuned."

ASH is broadly tuned at high concentrations and narrowly tuned at low concentrations (Fig. 4A), a pattern that might reflect its role as a nociceptor, mediating avoidance of any odorant when delivered at a sufficiently high concentration (Fig. 2, A to C). In previous behavioral experiments, most odorants in our panel were shown to be attractive at low concentrations and repulsive at high concentrations. A few odorants—1-heptanol, 1-octanol, and 1-nonanol—are repulsive at any tested concentration (table S2) (*35*). The odorants to which ASH is most sensitive are generally those that are repulsive at all concentrations.

The responses of each sensory neuron appear to occupy contiguous domains in chemical odor space. Each domain encompasses chemically similar odorant molecules that are effective stimuli for each sensory neuron (Fig. 4, B to E, and fig. S5). At high concentrations, broadly tuned neurons, such as AWA, extend responses throughout the chemical structure space. Even at high odorant concentrations, narrowly tuned neurons, such as ADF, extend responses over a smaller contiguous region of chemical space. This can be quantified as the average pairwise distance between the odors in odor space that significantly activate each neuron (Fig. 4G). Broadly tuned neurons span the entire space and therefore have the same average pairwise distance between odors as the baseline average pairwise distance of the entire odor panel. Narrowly tuned neurons have lower average pairwise distances—odors that activate narrowly tuned neurons are close to each other in odor space and are thus likely to be chemically similar.

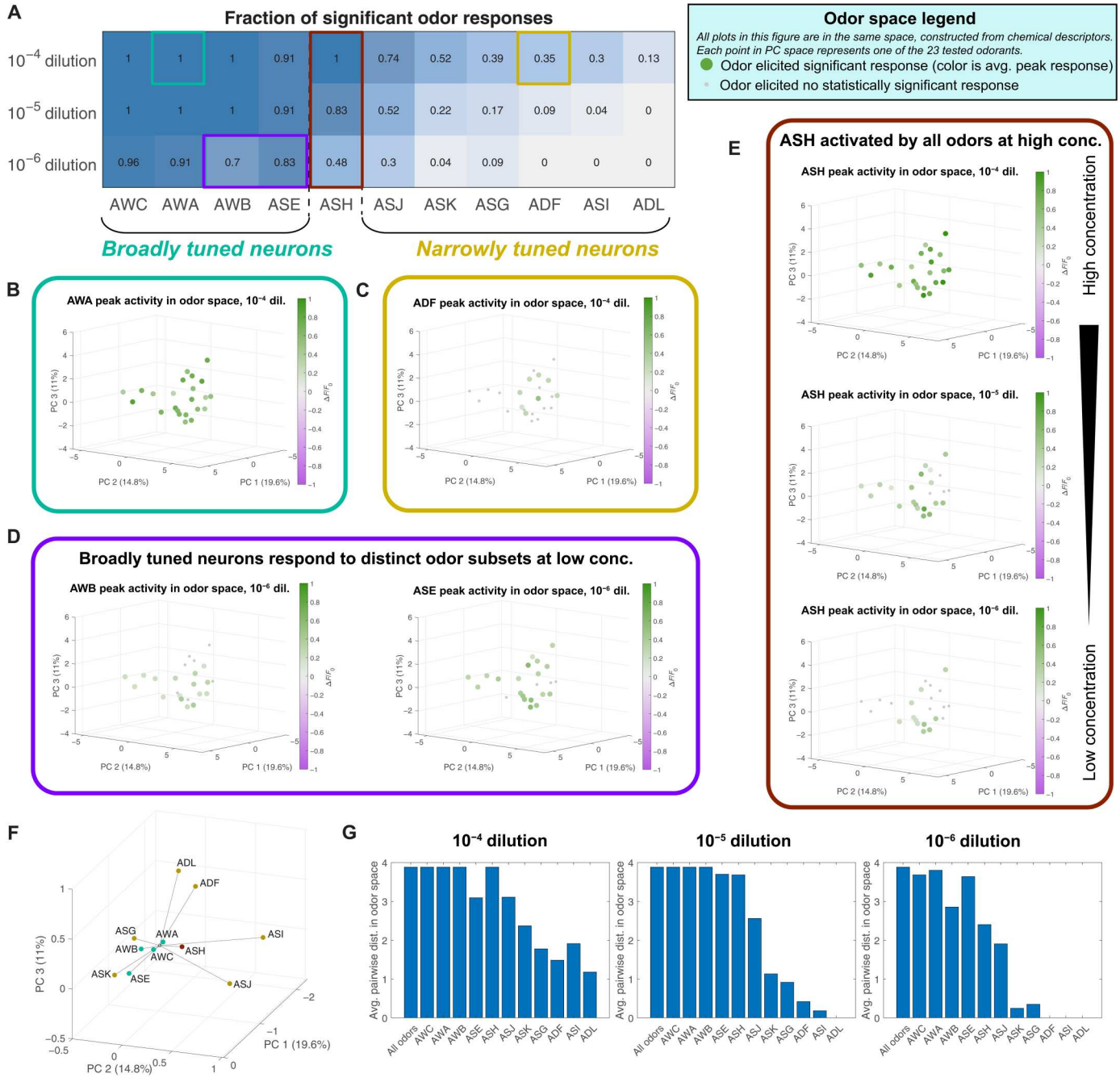

Fig. 4. Chemosensory neuron tuning. (**A**) Fraction of odorants in our 23-odor panel, which elicited significant responses ($q \leq 0.01$) in each neuron, at three different concentrations. We class neurons that responded to the majority of presented odors at high concentration as "broadly tuned" and neurons that responded to a small number of odors as "narrowly tuned." For each neuron, we plot peak responses to odorants in a space constructed from chemical descriptors (fig. S3A). (**B**) The activity of broadly tuned neurons (ex: AWA) spans this space, while (**C**) the activity of narrowly tuned neurons (ex: ADF) is confined to a subset of chemically similar odorants. (**D**) At low concentrations, broadly tuned neurons respond to distinct subsets of odorants. (**E**) ASH, a polymodal nociceptor, is activated by all tested odorants at high concentration but is only activated by a small set of repulsive odorants at low concentration. See fig. S5 for these plots for all neurons. (**F**) Centroids of the significant responses at 10^{-4} dilution of each neuron in odor space, weighted by the strength of each response. These centroids project in different directions from the center, suggesting that each neuron is most sensitive to a particular region of odor space. (**G**) Average pairwise distance between the odors that activate each neuron at high (left), medium (center), and low (right) concentrations, compared to the average pairwise distance between all 23 odors as a baseline. The broadly tuned neurons (AWC, AWA, AWB, ASE, and ASH) span most of the space, while the odors that activate narrowly tuned neurons (ASJ, ASK, ASG, ADF, ASI, and ADL) tend to be closer to each other on average and thus more similar in the chemical space.

Different sensory neurons can have overlapping response domains. However, each sensory neuron tends to be activated most strongly by a different part of odor space. We calculated the centroid of each neuron's activity in odor space, weighted by the strength of response to each odor and plotted relative to the center of our 23-odor panel (Fig. 4F). These activity centroids project in different directions from the center, suggesting that each neuron is most sensitive to a different region of odor space. The centroids of broadly tuned neurons are closer to center, as expected because they are activated by most odorants, and it is the weighting by response magnitude that pulls them off center. The centroids of narrowly tuned neurons are further from the center, as their significantly responding neurons occupy only one patch of odor space.

Most broadly tuned neurons extend responses over a smaller region of chemical space at lower concentrations than at high concentrations. Responses at low concentrations reveal the structural characteristics of molecules to which sensory neurons are most sensitive. AWA is most strongly activated by ketones, AWB is most strongly activated by esters, and ASE is most activated by alcohols (fig. S5). These regions of odor space are consistent with the directions to which the activity centroids of these neurons project at high concentration. ASH responds to odorants throughout chemical space, perhaps allowing ASH to contribute to the repellent response of any odorant delivered at sufficiently high concentration. The observation that each sensory neuron extends its sensitivity range across a contiguous region of chemical structural space suggests that each neuron is tuned to shared molecular properties of a set of odorant stimuli, as opposed to being tuned to exclusively detect specific odorants.

Single-trial responses suffice for discriminating odorant pairs

We observed trial-to-trial variability in odorant responses, both across animals and across odor presentations to the same animal. However, ensemble-level coding might confer robustness when discriminating odorants. We compiled all single-trial responses to each odorant across all datasets. In some recordings where data from individual neurons were missing, we imputed missing activity patterns using the rest of the ensemble (Appendix D and fig. S6, A to D). We used two dimensionality reduction methods to visualize the space spanned by single-trial responses—PCA and Uniform Manifold Approximation and Projection (UMAP). In a PC space constructed from the peak responses of all single trials, chemically similar odorants exhibit more similar representations (fig. S6D) and chemically dissimilar odorants exhibit dissimilar representations (fig. S6E). Overlap in a low-dimensional PC space is an imperfect measure for odorant discrimination because <60% of variance is explained by the first three principal components. Plotting all single-trial responses to all 23 odorants in UMAP space, trials for the same odorant also cluster together, although it is difficult to segregate trials for different odorants in this two-dimensional representation (Fig. 5A). Both PCA and UMAP analyses indicate that ensemble-level responses for the same odorant are similar. Both analyses also indicate that ensemble representations are high dimensional, as reduction to two or three dimensions removes a substantial fraction of the variance.

We asked whether olfactory representations were sufficiently dissimilar for reliable odorant discrimination based on single odorant presentations. To estimate the theoretical discriminability of odorant pairs, we computed errors in binary classification based on the pooled single-trial responses of each odorant pair using logistic regression (fig. S6F) and a support vector machine (fig. S6G). In all cases, binary classification succeeded with low error rate. Thus, any two odorants in our panel can be distinguished from each other on the basis of single-trial ensemble responses.

Odorant identification with single-trial responses

We asked whether odorant identity could reliably be decoded from single-trial ensemble responses, a task more challenging than binary classification of an odorant pair. We trained a multiclass classifier to perform linear discrimination (Fig. 5B). We randomly divided all single-trial measurements into a training set (90%) and validation (testing) set (10%). After we trained the classifier with the training set, we tested its performance in predicting odorant identities from single-trial measurements with the validation set (see Appendix E for details). This classifier successfully identified odorants in most of the single-trial measurements at high concentrations (Fig. 5C). Classification accuracy declined at lower concentrations but succeeded in the plurality of measurements (Fig. 5, D to F).

We used a similar approach to determine whether odorant intensity could be estimated from single-trial measurements. With trained multiclass classifiers, we were able to predict the concentration of a given odorant using single-trial measurements, although accuracy declined at lower concentrations (Fig. 5, G and H). In principle, the ensemble-level spatial map of sensory neuron activity contains sufficient information to determine odorant identity and intensity from single-stimulus presentations.

Virtual neuron knockouts degrade classifier accuracy

To quantify the relative contribution of each sensory neuron to ensemble-level discriminability, we performed virtual knockouts. We performed virtual knockouts by removing (masking) specific sensory neurons from the dataset and retraining the multiclass classifier on the remaining data. Removing any single sensory neuron led to small decreases in classification accuracy compared to wild type (Fig. 6, B to D). Classification accuracy was lower after masking narrowly tuned neurons (ASI, ASK, ASJ, or ASG) than broadly tuned neurons (AWA, ASH, or AWC).

Masking different neurons degrades the classification accuracy of a given odorant to different degrees. For instance, pentyl acetate is correctly classified 68% of the time when all 11 chemosensory neurons are included. ASJ masking reduces this accuracy to 62%, but AWA masking reduces accuracy to 48%. Masking any two neurons further decreases average classification accuracy (Fig. 6E). We computed the average classification accuracy when randomly removing different combinations of multiple neurons. We observed an inverse linear relationship between the number of masked neurons and classification accuracy (Fig. 6F). Odor identity across olfactory space is thus encoded in a distributed manner across all 11 chemosensory neurons.

Responses to pheromone stimuli are distinct from those of volatile odorants

All amphid chemosensory neurons respond to volatile odorants. We asked whether ensemble-level responses extend to other stimuli. *C. elegans* communicate using pheromones, a mixed group of glycolipid molecules called ascarosides (*24*, *29*). We presented young adult

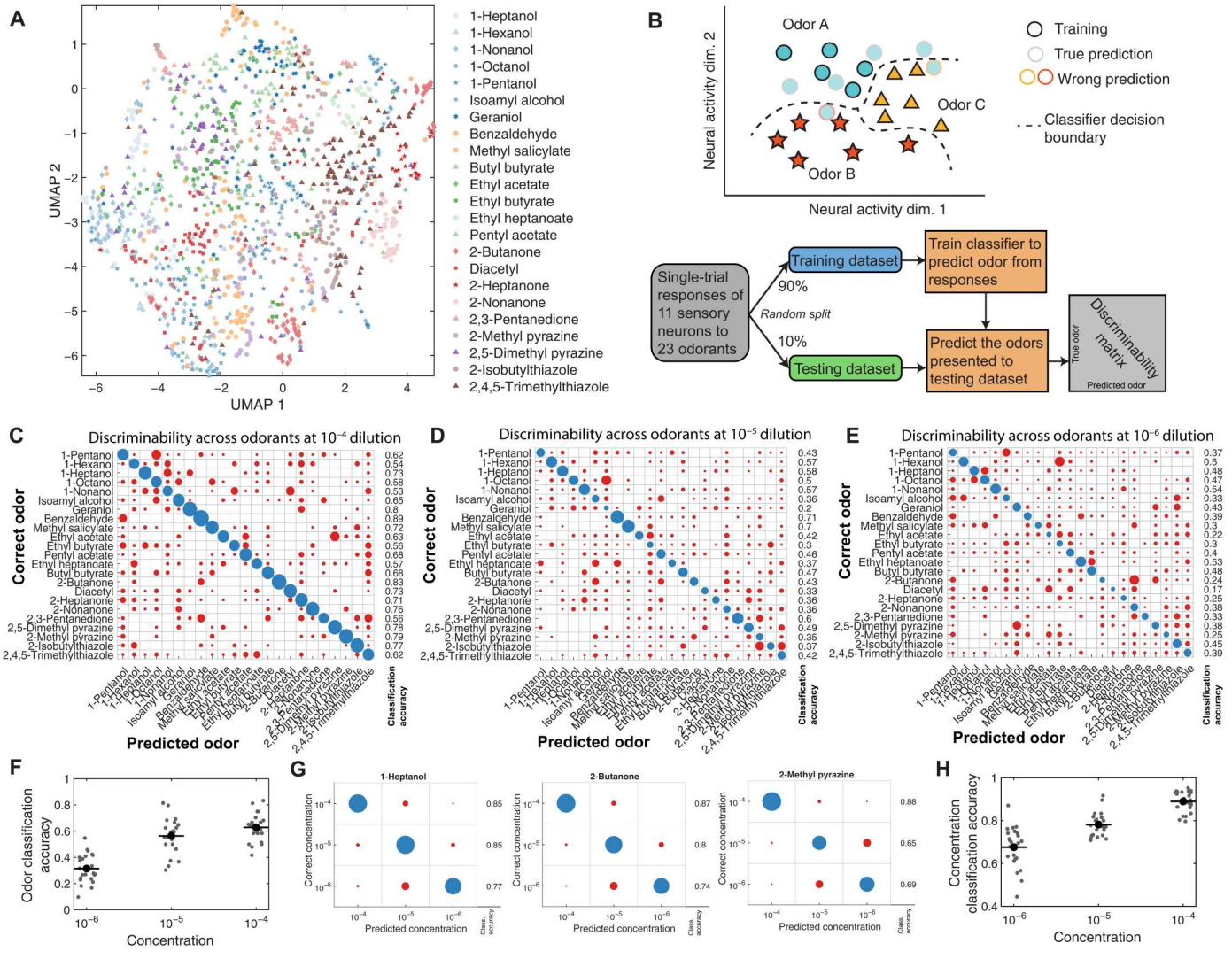

Fig. 5. Representative comparisons of single-trial odorant responses. (**A**) Low-dimensional UMAP representation of single-trial neural responses to all 23 odorants at 10^{-4} dilution. Responses to any given odorant generally cluster together. (**B**) Schematic of the multiclass classifier used for theoretical discriminability analysis of single-trial responses. The classifier was trained to predict odor identity from the peak responses of the ensemble of sensory neurons, generating a discriminability matrix. (**C**) Linear discriminability analysis of single-trial peak responses to high-concentration (10^{-4} dilution) odorants, with the presented odorant on the *y* axis and the classified odorant on the *x* axis. Circle size indicates the number of trials, with correct classifications colored blue and incorrect classifications colored red. The fraction of correctly classified trials for each odorant is to the right. Most of the single trials are correctly classified for each odorant. At lower concentrations, 10^{-5} dilution (**D**) and 10^{-6} dilution (**E**), classification accuracy diminishes. This is summarized in (**F**), a scatterplot of multiclass classification accuracy at different concentrations (C to E). (**G**) Within a given odorant (three examples shown), the concentration of the given odorant can be correctly classified on the basis of individual peak responses. (**H**) Across all odorants, concentration classification accuracy at different concentrations is shown.

hermaphrodites with a panel of five single ascarosides (#1, #2, #3, #5, and #8) (*25*).

Similarly to volatile odorants, ascarosides activated multiple sensory neurons (Fig. 7A). Some neurons—known to respond to ascarosides but narrowly tuned with respect to our volatile-odorant panel, such as ADL, ADF, and ASK—were strongly activated across our five-pheromone panel (Fig. 7B). Pheromones also evoked some activity in neurons that are broadly tuned to volatile odorants. For example, AWA was activated less often by the pheromone panel than by the odorant panel. Thus, pheromone detection may also involve an ensemble-level code, but a code that relies more heavily on those neurons that are narrowly tuned to volatile odorants.

DISCUSSION

In insects and vertebrates, the integrated activity of chemosensory neuron ensembles is often presumed to enhance odorant discrimination and broaden the space of olfactory perceptions with ensemble-level codes (*1*–*6*). The *C. elegans* olfactory system contains only 11 pairs of chemosensory neurons. Each nematode chemosensory neuron is considered a unique class distinguished by dendrite morphologies, wiring partners, and stimulus selectivity (*12*, *34*). Does

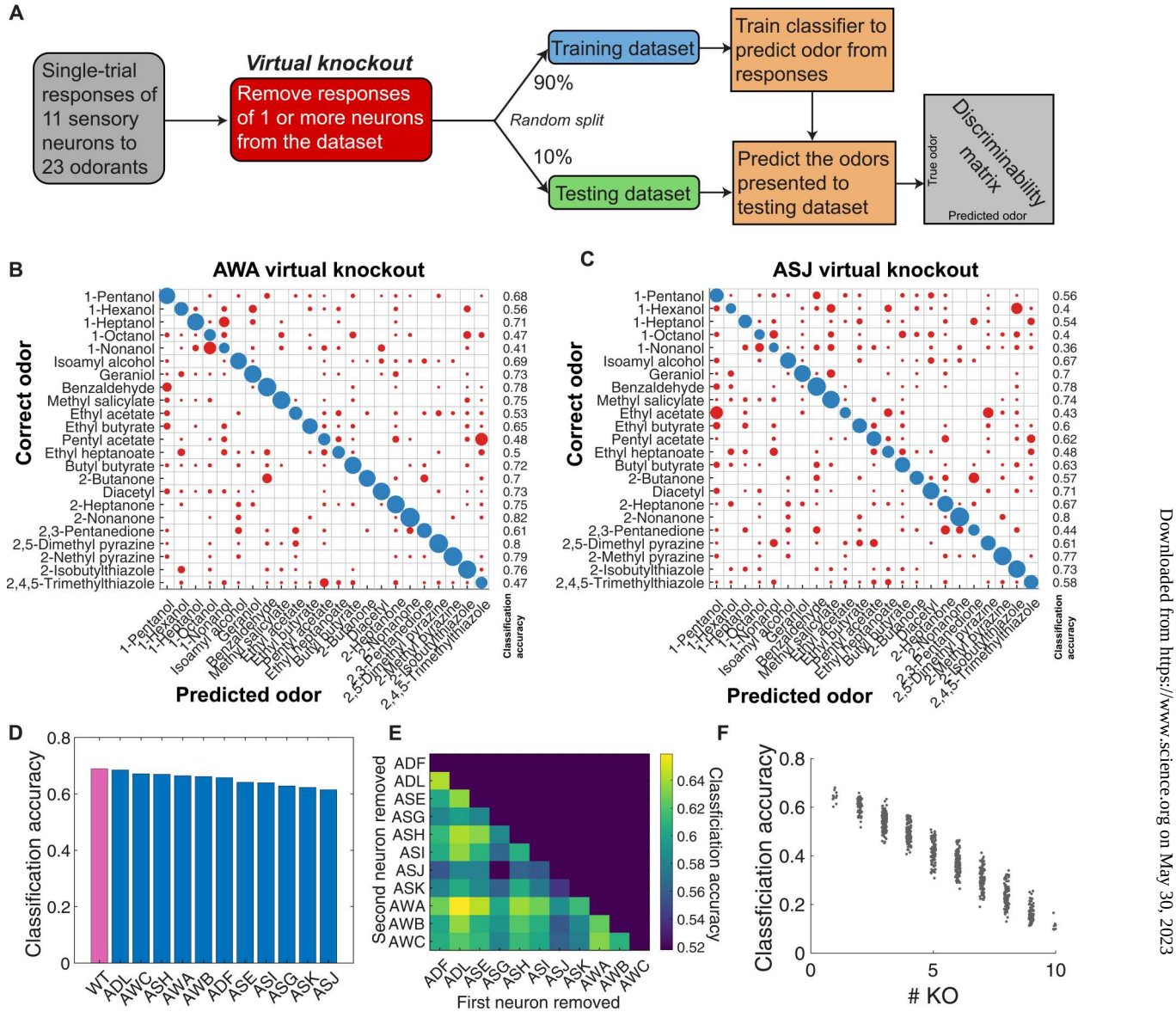

Fig. 6. Odorant discriminability is robust to virtual knockouts. (**A**) By removing the responses of one or more neurons from the dataset fed into the multiclass classifier, we assess the relative importance of different neurons to the theoretical discriminability of single-trial neural responses. Linear discriminability analysis of single-trial data, with (**B**) AWA or (**C**) ASJ virtually removed from the dataset. Removing different neurons changes the discriminability matrix in different ways. (**D**) We virtually removed each neuron from the dataset and computed the average classification accuracy for each virtual knockout (KO). Classification accuracy remains close to wild type (all 11 neurons) but is degraded more severely by removal of narrowly tuned neurons (ASI, ASK, ASJ, and ASG) than by removal of broadly tuned neurons. (**E**) Virtually removing pairs of neurons produces further reductions in average classification accuracy. (**F**) Plotting average classification accuracy of different sets of virtual knockouts reveals a linear relationship between theoretical classification accuracy and the number of chemosensory neurons.

the integrated activity of the *C. elegans* chemosensory ensemble contain information that might enhance and broaden olfactory discrimination?

We have simultaneously recorded calcium dynamics in all chemosensory neurons in nematodes exposed to a chemically diverse odorant panel. Nearly every distinct odorant stimulus evoked a distinct ensemble-level activity pattern among chemosensory neurons. We show that these highly reproducible ensemble-level patterns can, in principle, robustly encode odorant identity and intensity throughout a large chemical space.

Characterizing the ensemble-level olfactory code at the sensory periphery sets the stage for future studies aimed at their relevance for behavior and decision-making. Recording the activity of downstream interneurons will determine whether olfactory representations in circuits for behavior are similarly high dimensional, perhaps facilitating olfactory discrimination and diverse patterns of decision-making in complex environments.

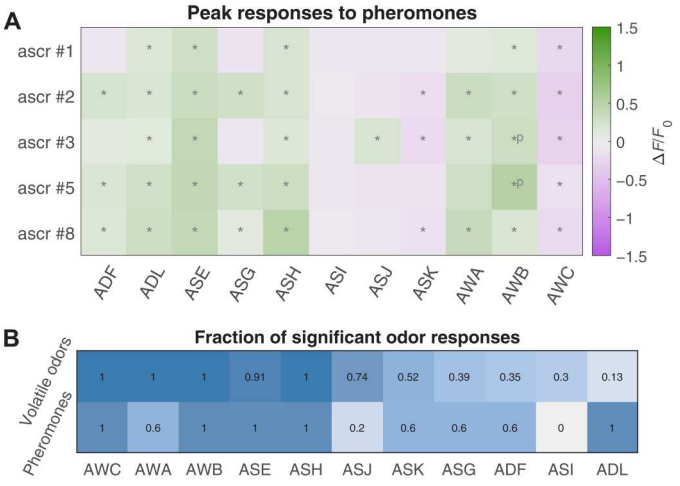

Fig. 7. Odorant representations of pheromones. (**A**) Average peak responses of the 11 chemosensory neurons to ascaroside pheromones #1, #2, #3, #5, and #8 at a concentration of 200 nM. Responses are reported as $\Delta F/F_0$, and significant responses ($q \leq 0.01$) are indicated with stars. (**B**) Fraction of volatile odorants (out of 23 odorants total), which elicited significant responses in each neuron at high concentration (first row), compared with the fraction of pheromone stimuli (out of five stimuli total), which elicited significant responses (second row). Many neurons (such as ADF and ADL) that are narrowly tuned with respect to volatile odorants appear to be activated more often by the ascaroside pheromones.

Diverse sensory neuron tuning properties

The unique response properties of the chemosensory neurons allow each to contribute information to the spatial activity map that encodes olfactory stimuli. Ensemble-level activity appears to be largely independent of synaptic communication between chemosensory neurons (Fig. 3B). Moreover, the tuning of each chemosensory neuron is shaped by the expression and properties of multiple receptors, not by the sensitivity of a single receptor, as is typical in larger animals. Removing any chemosensory neuron lowers the accuracy of stimulus classification based on ensemble-level activity (Fig. 6).

We lack comprehensive information about the expression patterns and odorant sensitivity of most olfactory receptors in *C. elegans*. ODR-10, highly expressed in AWA, remains the only characterized olfactory receptor for diacetyl (*38*, *53*). However, AWA also responds to many other odorants in a manner that is independent of ODR-10, evidence that AWA expresses additional receptors (*15*–*17*, *35*). Other sensory neurons that do not express ODR-10 are also activated by diacetyl at higher threshold concentrations. We uncovered a diversity of odorant dose-response curves to diacetyl and other odorants (Fig. 2E and fig. S3, F and G). This diversity is consistent with the expression of multiple receptors in each chemosensory neuron. Variable dose-response curves may reflect the cumulative activities of different sets of receptors with different binding affinities for each odorant across chemosensory neurons. Every chemosensory neuron tends to be sensitive to structurally similar odorants, suggesting that the receptors expressed by each neuron might be correlated in their chemical binding affinities (Fig. 4 and fig. S5).

Because we do not know the repertoire of odorant receptors that are expressed in each chemosensory neuron, we cannot easily characterize receptor-ligand interactions based on dose-response curves, as has been done in other animals (*4*, *62*, *63*). We note that the breadth of tuning to olfactory stimuli (defined as the fraction of the odor panel that elicit significant responses) is not strongly correlated with the number of expressed GPCRs (*13*). For example, ADL expresses the most GPCR genes of any chemosensory neuron but is sensitive to only three odorants in our panel. ASH, ASK, and ASJ express many GPCR genes, but only ASH is broadly tuned to our odorant panel. ASE, another broadly tuned neuron, expresses the smallest number of GPCR genes. Our inability to correlate the number of expressed GPCRs with the breadth of tuning might be because many GPCRs might not function as odorant receptors. For example, ADL, narrowly tuned for odorants but broadly tuned for pheromones, might use many GPCRs as ascaroside receptors.

Comparisons with olfactory systems in larger animals

In larger animals, chemosensory cells typically express single receptor types. In these animals, when domains of sensory neuron activity are represented in a chemical odor space, response domains tend to be clustered. Olfactory neuron ensembles span odor space by connecting the clustered response domains of different olfactory sensory neurons (*1*–*6*).

In *C. elegans*, each sensory neuron is sensitive to a contiguous region of chemical space (Fig. 4). This suggests that each neuron is tuned to shared molecular properties, as opposed to being faithful detectors of unique odorant molecules. The broad tuning of many *C. elegans* sensory neurons is probably caused by the combined activities of different receptors. Each receptor may be tuned to a given region of chemical structural space. Connecting the regions of chemical space corresponding to each receptor could produce the broad region of chemical space sensed by each neuron. The tendency for even the most broadly tuned neurons to be most strongly activated by certain chemical classes suggests correlations in the cell-specific expression of receptor types. The multireceptor nature of *C. elegans* sensory neurons may also contribute to their graded responses over broad concentration ranges. As additional receptor types with higher thresholds are recruited at higher concentrations of a given odorant, a sensory neuron gradually and cumulatively becomes more active.

The *C. elegans* chemosensory neuron ensemble-level activity encodes odorant identity

Previous studies in *C. elegans* largely dissected the properties of individual chemosensory neurons in response to selected odorants (*15*–*21*). For example, single olfactory sensory neurons can exhibit complex temporal activity patterns in response to odorant stimulation (*16*, *17*, *38*, *46*–*49*). Many previous studies have mapped the activities of single sensory neurons to behavioral outputs. However, using selected odorants to stimulate single sensory neurons and evoke behavioral responses does not reveal how olfactory inputs might be encoded by the sensory neuron ensemble.

We found that most olfactory stimuli activate multiple chemosensory neurons in *C. elegans* (Fig. 2). Chemosensory neurons that have been principally studied for roles in olfactory learning and navigation—AWA, AWB, AWC, and ASE—are the most broadly tuned, having high sensitivity to many different types of molecules. AWA is comparatively more strongly activated by ketones, AWB by some esters, and ASE by alcohols. AWC is

inhibited by every odorant that we tested. Other olfactory neurons —such as ASK, ASJ, or ASG—are more narrowly tuned, activated by a small number of structurally similar odorants (Fig. 4 and fig. S5). When ensemble-level responses of broadly and narrowly tuned chemosensory neurons are taken together, a reproducible and distinct spatial activity map emerges for each stimulus. This map encodes both odorant identity and intensity across the space spanned by our panel of 23 diverse chemicals at multiple concentrations (Fig. 5).

How might *C. elegans* use an ensemble-level code for olfaction? Broadly tuned neurons permit coarse identification of odorants. Each narrowly tuned neuron is sensitive to a smaller region of olfactory space. When a narrowly tuned neuron is active, the possible identities of each olfactory stimulus are limited to those odorant molecules inside its region of sensitivity. When a neuron is inactive, molecules inside its region of sensitivity are ruled out. Combinatorial activity patterns among chemosensory neurons with different regions of sensitivity can provide enough information to pinpoint the identity and concentration of an odorant stimulus. Because these ensemble-level patterns are highly reproducible, accurate discrimination can be performed with single-stimulus presentations. Ensemble-level codes may also improve robustness, compensating for trial-to-trial variability in the responses of individual chemosensory neurons.

We stress that showing that ensemble-level neuron activity is capable of encoding odorant identity and intensity throughout olfactory space does not necessarily mean that downstream circuits use this olfactory information in full when making behavioral decisions. Demonstrating that information is encoded at the sensory periphery sets the stage for future experiments to determine what part of this information is decoded for animal behavior.

Pheromone detection engages the chemosensory ensemble in distinct ways

We found that chemosensory neurons that are more narrowly tuned to volatile odorants are more broadly tuned to pheromones (Fig. 7). Activation of pheromone-sensing neurons by volatile odorants might reflect cross-reactivity of pheromone receptors to small organic molecules. These narrowly tuned neurons might also express different receptors with high odorant specificity. We also do not know whether the activation of broadly tuned olfactory neurons by pheromones reflects cross-reactivity of olfactory receptors to pheromone molecules. In any case, widespread ensemble-level activity across all chemosensory neurons in response to odorants and pheromones encodes substantial information that can be used to accurately identify any chemical stimulus.

Discrepancies with previously reported chemosensory responses

We have characterized >900 neuron-stimulus pairings, including many previously undescribed responses. Where our measurements overlapped with previous studies, we found general agreement with previously reported neuronal responses. However, we observed some discrepancies.

We did not observe previously reported OFF responses in AWC. There may be two reasons for this. First, to map the tuning properties of chemosensory neurons, we used stimulus conditions that would minimize adaptation. We presented odorants in short 10-s pulses with long intervening blank periods between presentations. Previously reported OFF responses in AWC were obtained with longer odor stimulus presentations (*15*, *37*). Second, some previously reported OFF responses were observed in one of the two asymmetric AWC neurons. Here, we did not separate the responses of AWC^{ON} and AWC^{OFF} neurons, and so any asymmetric AWC response would be lost in the population average.

We also did not observe some previously recorded sensory neuron responses to ascarosides (*26*–*29*). This might be due to differences in the age and sex of tested animals. To be consistent with our own volatile odorant experiments, we recorded from young adult hermaphrodites. Different ascaroside responses in previous reports were obtained using males and juvenile hermaphrodites.

Limitations and future studies

Calcium imaging is a coarse-grained measure of neuronal activity. We primarily quantified peak calcium responses, omitting differences in dynamics, spiking, or asymmetric responses, all of which likely encode additional information. Thus, our estimates of the information encoded in ensemble-level activity represent conservative lower bounds.

Our analysis of synaptic transmission mutants suggests that synaptic transmission is not the primary driver of ensemble-level responses (Fig. 3). Synaptic connections and feedback might shape the magnitude and dynamics of neuronal responses in important ways. For example, it has been suggested that feedback by neuropeptide signaling causes ASE to respond when benzaldehyde is detected by other sensory neurons (*17*). Nonsynaptic neurotransmitter signaling and electrical synapses might also coordinate activity among chemosensory neurons.

How does ensemble-level information relate to behavior? Many odorants studied in *C. elegans* have known behavioral valence: either attractive or repulsive to the animal (*35*). At high concentrations, many odorants become behaviorally repulsive. Do these switches in behavioral valence correlate with a change in the ensemble-level code? A simple prediction is that ASH activity increases as a stimulus becomes more repulsive. To understand changes in behavioral valence, it is necessary to simultaneously measure the ensemble-level olfactory code during decision-making in freely behaving animals. This is because it is difficult to calibrate previous experiments—where the behavioral valence of volatile odorants was determined with crawling animals on agar plates—with olfactory stimulation of immobilized worms using microfluidics.

Downstream from the chemosensory ensemble, interneuron networks resemble both a reflexive avoidance circuit (consisting of the premotor interneurons AVA, AVB, and AVD that primarily receive inputs from ASH) and a circuit for learning and navigation (consisting of the interneurons AIA, AIB, AIY, and AIZ that integrate the activity of the entire chemosensory ensemble) (Fig. 1A) (*10*, *30*, *31*, *33*, *36*, *39*, *64*, *65*). The activity of some of these interneurons is known to be modulated by differences in ensemble-level sensory neuron activity (*41*). ASH might be the start of a nociceptive reflex arc that maps the detection of noxious stimuli to rapid escape responses. The output of the entire chemosensory ensemble also appears to be integrated and decoded by another more complex interneuron network. Recently developed multineuronal recording methods (*21*, *66*, *67*) that extend from the chemosensory neurons to downstream interneurons might reveal how much olfactory information that is encoded at the sensory periphery is decoded in olfactory discrimination and behavioral decision-making.

We studied a broad panel of pure volatile odorants, all of which are known to elicit behavioral responses in the worm. In the natural environment of *C. elegans*, most olfactory cues will be mixtures of odorants, signifying diverse food sources or pathogens. Understanding how the chemosensory ensemble responds to these mixtures would illuminate ethologically relevant decision-making in downstream circuits.

The extent to which any animal exploits the collective activity of chemosensory neurons to decode olfactory inputs remains poorly understood. On one hand, the "dimensionality" of the olfactory code is often presumed to be as large as the number of distinct chemosensory neurons that contribute to the code (*68*). If so, the ability to detect even small numbers of different molecules, each with specificity to different chemosensory neurons, can create the potential to discriminate astronomical numbers of olfactory stimuli (*69*). On the other hand, animals might discard much of the high-dimensional olfactory information at the sensory periphery if it only needs to perform coarse categorizations of odorants such as "attractive" versus "repulsive." Rapid and efficient olfactory coding can be accomplished using only a small number of the earliest responding (or primary) olfactory receptors and neurons, as in recent experiments that explore "primacy models" of the olfactory code in rodents (*70*).

With advances in microfluidics and imaging technologies, it is becoming possible to combine high-throughput odorant stimulation with brain-wide imaging and tracking in behaving animals (*50*, *71*–*74*). With these tools, it will become possible to measure how much odorant information is decoded in behavioral discrimination tasks throughout the olfactory space that we characterized in this study. While the range of olfactory discrimination tasks and the combinatorial possibilities of the olfactory code are still large in *C. elegans*, its relatively small size makes it feasible to quantitatively assess the behavioral relevance of ensemble-level olfactory codes.

MATERIALS AND METHODS

Experimental design

The primary objective of the study was to understand how the 11 chemosensory neuron pairs in *C. elegans* encode odorant identity and intensity. We developed a transgenic nematode in which all of the ciliated sensory neurons were fluorescently labeled with GCaMP, allowing the activity of the 11 chemosensory neuron pairs to be recorded from simultaneously. We assembled a broad panel of 23 volatile odorants and five pheromones and used a microfluidic device to present these stimuli to nematodes. We used confocal microscopy to record from chemosensory neurons as odorant stimuli at multiple concentrations were presented.

Worm maintenance

All *C. elegans* lines used in this project were grown at 22°C on nematode growth medium plates seeded with the *Escherichia coli* strain OP50. All animal lines were allowed to recover from starvation or freezing for at least two generations before being used in experiments. All animals used in experiments were young adults.

Plasmids and crosses

To construct the ZM10104 imaging strain, we created and then crossed two integrated lines, one expressing GCaMP6s and one expressing the wCherry landmark. The first of these lines, ADS700, was made by coinjecting *lin-15(n765)* animals with pJH4039 (*ift-20* GCaMP6s::3xNLS) and a *lin-15*–rescuing plasmid. A stable transgenic line (hpEx3942) with consistent GCaMP expression in the chemosensory neurons was selected for integration, and transgenic animals were irradiated with ultraviolet (UV) light to integrate the transgenes into the genome. The resulting integrated line (aeaIs008) was backcrossed four times against N2 wild type. The second line, ADS701, was similarly made by coinjecting *lin-15(n765)* animals with pJH4040 (*gpc-1* wCherry) and a *lin-15*–rescuing plasmid. A stable transgenic line with good wCherry expression was selected for integration, and transgenic animals were irradiated with UV light to integrate the transgenes into the genome. The resulting integrated line (hpIs728) was backcrossed four times against N2 wild type. To make ZM10104, ADS700 hermaphrodites were crossed with N2 males. Heterozygous aeaIs008/+ male progeny were then crossed with ADS701 hermaphrodites. F1 progeny were picked for wCherry expression, and F2 progeny were picked for both GCaMP6s and wCherry expression. The line was then homozygozed in the F3 generation.

The ADS707 mutant imaging line was created by crossing the ZM10104 line with EG9631, an *unc-13(s69)* mutant obtained from the Caenorhabditis Genetics Center (CGC) (*53*). EG9631 hermaphrodites were crossed with ZM10104 males. Heterozygous (aeaIs008/+; hpIs728/+; +/*unc-13*) F1 hermaphrodite progeny were selected by GCaMP6s and wCherry expression and wild-type locomotion (*unc-13* is recessive). F2 progeny were picked for fluorescence and the *unc-13* uncoordinated phenotype. The line was homozygozed for fluorescence in the F3 generation.

Microfluidics

We used a modified version of a microfluidic system capable of delivering multiple odors to *Drosophila* larvae (*4*). The microfluidic chip is designed with an arbor containing delivery points for multiple stimuli, together with a buffer delivery point and two control switches, one for buffer and one for odor (Fig. 1B). At any given time, three flows are active: one of the control switches, the buffer blank, and one odor stimulus. The chip is designed to maintain laminar flow of each fluid, and the flow is split between a waste channel and an odor channel, which flows past the animal's nose. The chip described here is designed to switch rapidly from one stimulus to the buffer. After the flows pass the animal, they exit the chip via a waste port at atmospheric pressure. Waste is removed with a vacuum.

We grafted the odorant delivery arbor to a *C. elegans* loading chamber similar to those designed by Chronis *et al.* (*55*). We designed a loading chamber suitable for adult *C. elegans*, a narrow channel 62 μm wide and 30 μm high, with a gently tapered end. The tapered end serves as a guide to help hold the animal's nose in place without distorting the animal. The microfluidic device pattern was designed in AutoCAD, and the design was translated to silicon wafer using photolithography. The photomasks of the design were printed using CAD/Art Services Inc. The silicon wafer was then used as a mold for polydimethylsiloxane (PDMS) to fabricate microfluidic devices. The PDMS components were then removed from the silicon wafer, cut to size, and had access channels made with a biopsy punch. The completed PDMS components were then plasma-bonded to no. 1 glass cover slips. To minimize contamination from dust, all microfluidics assembly was done in a cleanroom.

Preparation of odorant and buffer solutions

Odorants were diluted in CTX buffer (5 mM KH_2PO_4/K_2HPO_4 at pH 6, 1 mM $CaCl_2$, 1 mM $MgSO_4$, and 50 mM NaCl, adjusted to 350 mOsm/liter with sorbitol). To prevent contamination, each odor condition was mixed and stored in its own glass bottle and delivered through its own glass syringe and tubing. Furthermore, a new microfluidic device was used for a single consistent panel of odors. The single ascarosides (*25*) were diluted in CTX buffer to 200 mM concentration for presentation to the animals.

Stimulus delivery protocol

We chose to deliver 10-s odorant pulses separated by 30-s buffer blanks. These pulse and blank lengths were sufficiently spaced to elicit similar neuronal responses across pulses, with no indication of adaptation (fig. S2, A and B). We carried out control experiments by presenting each animal in the microfluidic device with multiple conditions (odorants and concentrations) in a single trial (fig. S2, C and D). Randomizing the order of odorant delivery, we did not observe any effects of odorant order on the responses of the sensory neurons.

We previously used a similar stimulus protocol by Yemini *et al.* (*21*), presenting three chemosensory stimuli separated by buffer blanks in a randomized order. There, we similarly observed no differences in average odorant-evoked responses that were correlated with odorant delivery order.

Thus, to reduce the risk of odorant cross-contamination, we elected to conduct the remaining experiments by presenting each animal with multiple presentations of one stimulus condition (fig. S2, A and B) and averaged across the population of at least 10 animals per condition, treating the response to each odorant pulse response as an independent trial.

Imaging setup

We used a single-photon, spinning-disk confocal microscope to capture fluorescent images from intact *C. elegans*. The microscope was inverted to allow for easy access to the microfluidic device mounted on the stage. We used a 488-nm laser to excite GCaMP in vivo and used a 561-nm laser to excite the wCherry landmark. To minimize cross-talk between channels, lasers were fired sequentially during multicolor recordings. We captured images with a 60× water-immersion objective with a numerical aperture of 1.2. Volumes were acquired using unidirectional scans of a piezo objective scanner. All fluorescence microscopy is a trade-off between spatial resolution, temporal resolution, laser power, and signal strength. We optimized two sets of imaging conditions, one set for activity imaging and another set for landmark imaging. Both sets of imaging conditions capture the region containing most of the neurons in the head of *C. elegans*, a volume of 112 μm by 56 μm by 30 μm.

In any given experiment, acquisition of a landmark volume precedes acquisition of an activity movie. This volume, which contains both green and red channels, allows us to identify neurons of interest. The spatial resolution of these volumes is 0.5 μm by 0.5 μm by 1.5 μm per voxel, with the z-resolution of 1.5-μm set by the point spread function.

The activity movies were acquired at a high speed in the green channel only, with lower spatial resolution (1 μm by 1 μm by 1.5 μm per voxel). At this resolution, we could acquire volumes at 2.5 Hz in standard acquisition mode.

Analyzing multineuronal recordings

The neurons in each activity recording were identified and then tracked through time using a neighborhood correlation tracking method. The criteria for identifying each neuron class are described in the Supplementary Methods. Neurons that could not be unambiguously identified were excluded from the dataset. All neuron tracks were then manually proofread to exclude mistracked neurons. Activity traces were bleach-corrected and reported in $\Delta F/F_0 = [F(t) - F_0]/F_0$. Normalization by baseline fluorescence F_0 allowed for direct comparisons within a given neuron class across left and right sides and across individuals. The baseline F_0 value was determined individually for every recorded neuron, set at the fifth percentile of the distribution of bleach-corrected fluorescence values, with the opportunity for manual correction.

Statistical analysis

We used two-tailed, paired *t* tests to compare the mean signal during stimulus presentation with an unstimulated period of identical length within the same neuron. Neurons were tested for both ON and OFF responses. The *P* values were corrected for multiple testing using false discovery rate (*76*). To test for asymmetric neuron responses, we used two-tailed, two-sample *t* tests (unpaired). Sensory neuron responses to all conditions are publicly available at this data repository, together with plots of average responses, phase trajectories, and time trace correlation matrices.

Supplementary Materials

This PDF file includes:

Supplementary Methods
Figs. S1 to S6
Tables S1 and S2
References

View/request a protocol for this paper from *Bio-protocol*.

REFERENCES AND NOTES

1. B. Malnic, J. Hirono, T. Sato, L. B. Buck, Combinatorial receptor codes for odors. *Cell* **96**, 713–723 (1999).
2. K. Nara, L. R. Saraiva, X. Ye, L. B. Buck, A large-scale analysis of odor coding in the olfactory epithelium. *J. Neurosci.* **31**, 9179–9191 (2011).
3. S. A. Kreher, D. Mathew, J. Kim, J. R. Carlson, Translation of sensory input into behavioral output via an olfactory system. *Neuron* **59**, 110–124 (2008).
4. G. Si, J. K. Kanwal, Y. Hu, C. J. Tabone, J. Baron, M. Berck, G. Vignoud, A. D. T. Samuel, Structured odorant response patterns across a complete olfactory receptor neuron population. *Neuron* **101**, 950–962.e7 (2019).
5. J. W. Wang, A. M. Wong, J. Flores, L. B. Vosshall, R. Axel, Two-photon calcium imaging reveals an odor-evoked map of activity in the fly brain. *Cell* **112**, 271–282 (2003).
6. E. A. Hallem, J. R. Carlson, Coding of odors by a receptor repertoire. *Cell* **125**, 143–160 (2006).
7. J. del Marmol, M. A. Yedlin, V. Ruta, The structural basis of odorant recognition in insect olfactory receptors. *Nature* **597**, 126–131 (2021).
8. M. De Bruyne, T. C. Baker, Odor detection in insects: Volatile codes. *J. Chem. Ecol.* **34**, 882–897 (2008).
9. P. S. Grewal, D. J. Wright, Migration of *Caenorhabditis elegans* larvae towards bacteria and the nature of the bacterial stimulus. *Fundam. Appl. Nematol.* **15**, 159–166 (1992).
10. C. I. Bargmann, H. Robert Horvitz, Chemosensory neurons with overlapping functions direct chemotaxis to multiple chemicals in *C. elegans*. *Neuron* **7**, 729–742 (1991).
11. C. I. Bargmann, Comparative chemosensation from receptors to ecology. *Nature* **444**, 295–301 (2006).
12. C. I. Bargmann, Chemosensation in *C. elegans*, *WormBook: The Online Review of C. elegans Biology* (2006), pp. 1–29; 10.1895/wormbook.1.123.1.

13. B. Vidal, U. Aghayeva, H. Sun, C. Wang, L. Glenwinkel, E. A. Bayer, O. Hobert, An atlas of *Caenorhabditis elegans* chemoreceptor expression. *PLOS Biol.* **16**, 1–34 (2018).
14. L. A. Perkins, E. M. Hedgecock, J. N. Thomson, J. G. Culotti, Mutant sensory cilia in the nematode *Caenorhabditis elegans*. *Dev. Biol.* **117**, 456–487 (1986).
15. K. Yoshida, T. Hirotsu, T. Tagawa, S. Oda, T. Wakabayashi, Y. Iino, T. Ishihara, Odour concentration-dependent olfactory preference change in *C. elegans*. *Nat. Commun.* **3**, 739 (2012).
16. J. Larsch, D. Ventimiglia, C. I. Bargmann, D. R. Albrecht, High-throughput imaging of neuronal activity in *Caenorhabditis elegans*. *Proc. Natl. Acad. Sci. U.S.A.* **110**, E4266–E4273 (2013).
17. S. G. Leinwand, C. J. Yang, D. Bazopoulou, N. Chronis, J. Srinivasan, S. H. Chalasani, Circuit mechanisms encoding odors and driving aging-associated behavioral declines in *Caenorhabditis elegans*. *eLife* **4**, e10181 (2015).
18. A. Zaslaver, I. Liani, O. Shtangel, S. Ginzburg, L. Yee, P. W. Sternberg, Hierarchical sparse coding in the sensory system of *Caenorhabditis elegans*. *Proc. Natl. Acad. Sci. U.S.A.* **112**, 1185–1189 (2015).
19. S. Yu, L. Avery, E. Baude, D. L. Garbers, Guanylyl cyclase expression in specific sensory neurons: A new family of chemosensory receptors. *Proc. Natl. Acad. Sci. U. S. A.* **94**, 3384–3387 (1997).
20. P. D. Wes, C. I. Bargmann, *C. elegans* odour discrimination requires asymmetric diversity in olfactory neurons. *Nature* **410**, 698–701 (2001).
21. E. Yemini, A. Lin, A. Nejatbakhsh, E. Varol, R. Sun, G. E. Mena, A. D. T. Samuel, L. Paninski, V. Venkatachalam, O. Hobert, NeuroPAL: A multicolor atlas for whole-brain neuronal identification in *C. elegans*. *Cell* **184**, 272–288, 288.e11 (2021).
22. T. R. Thiele, S. Faumont, S. R. Lockery, The neural network for chemotaxis to tastants in *Caenorhabditis elegans* is specialized for temporal differentiation. *J. Neurosci.* **23**, 11904–11911 (2005).
23. H. Suzuki, T. R. Thiele, S. Faumont, M. Ezcurra, S. R. Lockery, W. R. Schafer, Functional asymmetry in *Caenorhabditis elegans* taste neurons and its computational role in chemotaxis. *Nature* **454**, 114–117 (2008).
24. E. Z. MacOsko, N. Pokala, E. H. Feinberg, S. H. Chalasani, R. A. Butcher, J. Clardy, C. I. Bargmann, A hub-and-spoke circuit drives pheromone attraction and social behaviour in *C. elegans*. *Nature* **458**, 1171–1175 (2009).
25. A. Narayan, V. Venkatachalam, O. Durak, D. K. Reilly, N. Bose, F. C. Schroeder, A. D. T. Samuel, J. Srinivasan, P. W. Sternberg, Contrasting responses within a single neuron class enable sex-specific attraction in *Caenorhabditis elegans*. *Proc. Natl. Acad. Sci. U.S.A.* **113**, E1392–E1401 (2016).
26. J. S. Greene, M. Brown, M. Dobosiewicz, I. G. Ishida, E. Z. Macosko, X. Zhang, R. A. Butcher, D. J. Cline, P. T. McGrath, C. I. Bargmann, Balancing selection shapes density-dependent foraging behaviour. *Nature* **539**, 254–258 (2016).
27. E. Z. Aprison, I. Ruvinsky, Counteracting ascarosides act through distinct neurons to determine the sexual identity of *C. elegans* pheromones. *Curr. Biol.* **27**, 2589–2599.e3 (2017).
28. K. A. Fagan, J. Luo, R. C. Lagoy, F. C. Schroeder, D. R. Albrecht, D. S. Portman, A single-neuron chemosensory switch determines the valence of a sexually dimorphic sensory behavior. *Curr. Biol.* **28**, 902–914.e5 (2018).
29. P. T. McGrath, I. Ruvinsky, A primer on pheromone signaling in *Caenorhabditis elegans* for systems *biologists*. *Curr. Opin. Syst. Biol.* **13**, 23–30 (2019).
30. M. A. Hilliard, C. I. Bargmann, P. Bazzicalupo, *C. elegans* responds to chemical repellents by integrating sensory inputs from the head and the tail. *Curr. Biol.* **12**, 730–734 (2002).
31. M. A. Hilliard, C. Bergamasco, S. Arbucci, R. H. A. Plasterk, P. Bazzicalupo, Worms taste bitter: ASH neurons, QUI-1, GPA-3 and ODR-3 mediate quinine avoidance in *Caenorhabditis elegans*. *EMBO J.* **23**, 1101–1111 (2004).
32. J. M. Kaplan, H. R. Horvitz, A dual mechanosensory and chemosensory neuron in *Caenorhabditis elegans*. *Proc. Natl. Acad. Sci. U.S.A.* **90**, 2227–2231 (1993).
33. Y. Sambongi, T. Nagae, Y. Liu, T. Yoshimizu, K. Takeda, Y. Wada, M. Futai, Sensing of cadmium and copper ions by externally exposed ADL, ASE, and ASH neurons elicits avoidance response in *Caenorhabditis elegans*. *Neuroreport* **10**, 753–757 (1999).
34. A. Metaxakis, D. Petratou, N. Tavernarakis, Multimodal sensory processing in *Caenorhabditis elegans*. *Open Biol.* **8**, (2018).
35. C. I. Bargmann, E. Hartwieg, H. R. Horvitz, Odorant-selective genes and neurons mediate olfaction in *C. elegans*. *Neuron* **74**, 515–527 (1993).
36. S. H. Chalasani, N. Chronis, M. Tsunozaki, J. M. Gray, D. Ramot, M. B. Goodman, C. I. Bargmann, Erratum: Dissecting a circuit for olfactory behaviour in *Caenorhabditis elegans*. *Nature* **451**, 63–70 (2008).
37. M. Tsunozaki, S. H. Chalasani, C. I. Bargmann, A behavioral switch: cgmp and pkc signaling in olfactory neurons reverses odor preference in *C. elegans*. *Neuron* **59**, 959–971 (2008).
38. E. R. Troemel, B. E. Kimmel, C. I. Bargmann, Reprogramming chemotaxis responses: Sensory neurons define olfactory preferences in *C. elegans*. *Cell* **91**, 161–169 (1997).
39. H.-i. Ha, M. Hendricks, Y. Shen, C. V. Gabel, C. Fang-Yen, Y. Qin, D. Colón-Ramos, K. Shen, A. D. T. Samuel, Y. Zhang, Functional organization of a neural network for aversive olfactory learning in *Caenorhabditis elegans*. *Neuron* **68**, 1173–1186 (2010).
40. D. Cheng, J. S. Lee, M. Brown, M. S. Ebert, P. T. McGrath, M. Tomioka, Y. Iino, C. I. Bargmann, Insulin/igf signaling regulates presynaptic glutamate release in aversive olfactory learning. *Cell Rep.* **41**, 111685 (2022).
41. M. Dobosiewicz, Q. Liu, C. I. Bargmann, Reliability of an interneuron response depends on an integrated sensory state. *eLife* **8**, e50566 (2019).
42. H. A. Colbert, C. I. Bargmann, Odorant-specific adaptation pathways generate olfactory plasticity in *C. elegans*. *Neuron* **14**, 803–812 (1995).
43. N. D. L'Etoile, C. M. Coburn, J. Eastham, A. Kistler, G. Gallegos, C. I. Bargmann, The cyclic GMP-dependent protein kinase EGL-4 regulates olfactory adaptation in *C. elegans*. *Neuron* **36**, 1079–1089 (2002).
44. G. Jansen, D. Weinkove, R. H. A. Plasterk, The G-protein γ subunit gpc-1 of the nematode *C. elegans* is involved in taste adaptation. *EMBO J.* **21**, 986–994 (2002).
45. M. A. Hilliard, A. J. Apicella, R. Kerr, H. Suzuki, P. Bazzicalupo, W. R. Schafer, In vivo imaging of *C. elegans* ASH neurons: Cellular response and adaptation to chemical repellents. *EMBO J.* **24**, 63–72 (2005).
46. S. Levy, C. I. Bargmann, An adaptive-threshold mechanism for odor sensation and animal navigation. *Neuron* **105**, 534–548.e13 (2020).
47. M. Khan, A. H. Hartmann, M. P. O'Donnell, M. Piccione, A. Pandey, P.-H. Chao, N. D. Dwyer, C. I. Bargmann, P. Sengupta, Context-dependent reversal of odorant preference is driven by inversion of the response in a single sensory neuron type. *PLOS Biol.* **20**, e3001677 (2022).
48. Q. Liu, P. B. Kidd, M. Dobosiewicz, C. I. Bargmann, *C. elegans* AWA olfactory neurons fire calcium-mediated all-or-none action potentials. *Cell* **175**, 57–70.e17 (2018).
49. I. G McLachlan, T. S. Kramer, M. Dua, E. M. Diloreto, U. Dag, J. Srinivasan, S. W. Flavell, Diverse states and stimuli tune olfactory receptor expression levels to modulate food-seeking behavior. bioRxiv 2022.04.27.489714 [**Preprint**]. 28 April 2022. https://doi.org/10.1101/2022.04.27.489714.
50. N. Chronis, M. Zimmer, C. I. Bargmann, Microfluidics for in vivo imaging of neuronal and behavioral activity in *Caenorhabditis elegans*. *Nat. Methods* **4**, 727–731 (2007).
51. S. E. Worthy, L. Haynes, M. Chambers, D. Bethune, E. Kan, K. Chung, R. Ota, C. J. Taylor, E. E. Glater, Identification of attractive odorants released by preferred bacterial food found in the natural habitats of *C. elegans*. *PLOS ONE* **13**, 1–14 (2018).
52. R. Haddad, R. Khan, Y. K. Takahashi, K. Mori, D. Harel, N. Sobel, A metric for odorant comparison. *Nat. Methods* **5**, 425–429 (2008).
53. P. Sengupta, J. H. Chou, C. I. Bargmann, odr-10 Encodes a seven transmembrane domain olfactory receptor required for responses to the odorant diacetyl. *Cell* **84**, 899–909 (1996).
54. P. J. Summers, R. M. Layne, A. C. Ortega, G. P. Harris, B. A. Bamber, R. W. Komuniecki, Multiple sensory inputs are extensively integrated to modulate nociception in *C. elegans*. *J. Neurosci.* **35**, 10331–10342 (2015).
55. J. G. White, E. Southgate, J. N. Thomson, S. Brenner, The structure of the nervous system of the nematode *Caenorhabditis elegans*. *Philos. Trans. R. Soc. Lond. B Biol. Sci.* **314**, 1–340 (1986).
56. D. Witvliet, B. Mulcahy, J. K. Mitchell, Y. Meirovitch, D. R. Berger, Y. Wu, Y. Liu, W. X. Koh, R. Parvathala, D. Holmyard, R. L. Schalek, N. Shavit, A. D. Chisholm, J. W. Lichtman, A. D. T. Samuel, M. Zhen, Connectomes across development reveal principles of brain maturation. *Nature* **596**, 257, 261 (2021).
57. J. E. Richmond, W. S. Davis, E. M. Jorgensen, UNC-13 is required for synaptic vesicle fusion in *C. elegans*. *Nat. Neurosci.* **2**, 959–964 (1999).
58. H. Sass, Sensory encoding of odor stimuli in *Periplaneta americana*. *J. Comp. Physiol. A Neuroethol. Sens. Neural Behav. Physiol.* **107**, 49–65 (1976).
59. M. Meister, T. Bonhoeffer, Tuning and topography in an odor map on the rat olfactory bulb. *J. Neurosci.* **21**, 1351–1360 (2001).
60. H. Saito, Q. Chi, H. Zhuang, H. Matsunami, J. D. Mainland, Odor coding by a mammalian receptor repertoire. *Sci. Signal.* **2**, ra9 (2009).
61. D. Zwicker, A. Murugan, M. P. Brenner, Receptor arrays optimized for natural odor statistics. *Proc. Natl. Acad. Sci. U.S.A.* **113**, 5570–5575 (2016).
62. S. Qin, Q. Li, C. Tang, Y. Tu, Optimal compressed sensing strategies for an array of nonlinear olfactory receptor neurons with and without spontaneous activity. *Proc. Natl. Acad. Sci. U.S.A.* **116**, 20286–20295 (2019).
63. K. Kajiya, K. Inaki, M. Tanaka, T. Haga, H. Kataoka, K. Touhara, Molecular bases of odor discrimination: Reconstitution of olfactory receptors that recognize overlapping sets of odorants. *J. Neurosci.* **21**, 6018–6025 (2001).
64. H. Spors, M. Wachowiak, L. B. Cohen, R. W. Friedrich, Temporal dynamics and latency patterns of receptor neuron input to the olfactory bulb. *J. Neurosci.* **26**, 1247–1259 (2006).
65. T. Wakabayashi, I. Kitagawa, R. Shingai, Neurons regulating the duration of forward locomotion in *Caenorhabditis elegans*. *Neurosci. Res.* **50**, 103–111 (2004).

66. P. A. Garrity, M. B. Goodman, A. D. Samuel, P. Sengupta, Running hot and cold: Behavioral strategies, neural circuits, and the molecular machinery for thermotaxis in C. *elegans* and *Drosophila*. *Genes Dev.* **24**, 2365–2382 (2010).
67. H. S. Kaplan, M. Zimmer, Brain-wide representations of ongoing behavior: A universal principle? *Curr. Opin. Neurobiol.* **64**, 60–69 (2020).
68. A. Lin, D. Witvliet, L. Hernandez-Nunez, S. W. Linderman, A. D. T. Samuel, V. Venkatachalam, Imaging whole-brain activity to understand behaviour. *Nat. Rev. Phys.* **4**, 292–305 (2022).
69. M. Meister, On the dimensionality of odor space. *eLife* **4**, e07865 (2015).
70. C. Bushdid, M. O. Magnasco, L. B. Vosshall, A. Keller, Humans can discriminate more than 1 trillion olfactory stimuli. *Science* **343**, 1370–1372 (2014).
71. C. D. Wilson, G. O. Serrano, A. A. Koulakov, D. Rinberg, A primacy code for odor identity. *Nat. Commun.* **8**, 1477 (2017).
72. D. R. Albrecht, C. I. Bargmann, High-content behavioral analysis of *Caenorhabditis elegans* in precise spatiotemporal chemical environments. *Nat. Methods* **8**, 599–605 (2011).
73. J. P. Nguyen, A. N. Linder, G. S. Plummer, J. W. Shaevitz, A. M. Leifer, Automatically tracking neurons in a moving and deforming brain. *PLOS Comput. Biol.* **13**, e1005517 (2017).
74. V. Venkatachalam, N. Ji, X. Wang, C. Clark, J. K. Mitchell, M. Klein, C. J. Tabone, J. Florman, H. Ji, J. Greenwood, A. D. Chisholm, J. Srinivasan, M. Alkema, M. Zhen, A. D. T. Samuel, Pan-neuronal imaging in roaming *Caenorhabditis elegans*. *Proc. Natl. Acad. Sci. U.S.A.* **113**, E1082–E1088
75. K. M. Hallinen, R. Dempsey, M. Scholz, X. Yu, A. Linder, F. Randi, A. K. Sharma, J. W. Shaevitz, A. M. Leifer, Decoding locomotion from population neural activity in moving *C. elegans*. *eLife* **10**, e66135 (2021).
76. J. D. Storey, A direct approach to false discovery rates. *J. R. Stat. Soc. B* **64**, 479–498 (2002).
77. E. Candès, B. Recht, Exact matrix completion via convex optimization. *Commun. ACM* **55**, 111–119 (2012).
78. L. T. Nguyen, J. Kim, B. Shim, Low-rank matrix completion: A contemporary survey. *IEEE Access* **7**, 94215–94237 (2019).
79. J. Fan, L. Ding, Y. Chen, M. Udell, Factor group-sparse regularization for efficient low-rank matrix recovery. *Adv. Neural Inf. Process. Syst.* **32**, (2019).
80. M. Linkert, C. T. Rueden, C. Allan, J. M. Burel, W. Moore, A. Patterson, B. Loranger, J. Moore, C. Neves, D. M. Donald, A. Tarkowska, C. Sticco, E. Hill, M. Rossner, K. W. Eliceiri, J. R. Swedlow, Metadata matters: Access to image data in the real world. *J. Cell Biol.* **189**, 777–782 (2010).
81. P. Kovesi, Good colour maps: How to design them. arXiv:1509.03700 [cs.GR] (12 September 2015).

Acknowledgments: We thank G. Si and J. Kanwal for advice on microfluidics design and operation and M. Seyedolmohadesin and M. Torkashvand for discussions on ascaroside responses. We also thank S. R. Datta, S. Flavell, and the members of the Zhen, Pehlevan, and Samuel laboratories for advice on the project and comments on the manuscript. The EG9631 strain was obtained from the CGC, which is funded by the NIH Office of Research Infrastructure Programs (P40 OD010440). Microfluidic devices were manufactured using the Soft Materials Cleanroom facility of the Harvard MRSEC (DMR-1420570). **Funding:** This work was supported by NSF Brain Eager NSF IOS-1452593 (to A.D.T.S.), NSF Physics of Living Systems NSF 1806818 (to A.L. and A.D.T.S.), NSF Ideas NSF IOS-1555914 (to A.D.T.S.), NIH Brain Initiative NIH 1UF1NS111697-01 (to C.P., A.D.T.S., and M.Z.), Burroughs Wellcome Fund Career Award at the Scientific Interface (to V.V.), and Canadian Institutes of Health Research CIHR Foundation Scheme 154274 (to M.Z.). **Author contributions:** Conceptualization: A.L., V.V., M.Z., and A.D.T.S. Genetics and reagents: A.L., M.W., L.L., W.H., and M.Z. Experimental setup design and build: A.L. and V.V. Software: A.L. and V.V. Imaging experiments: A.L., H.C., G.C., N.Z.T., and R.V. Analysis and modeling: A.L. and S.Q. Supervision: C.P., M.Z., and A.D.T.S. Writing—original draft: A.L., V.V., M.Z., and A.D.T.S. Writing—review and editing: S.Q., H.C., and C.P. **Competing interests:** The authors declare that they have no competing interests. **Data and materials availability:** All data needed to evaluate the conclusions in the paper are present in the paper and/or the Supplementary Materials. The animal strains used in this study are available at the CGC (https://cgc.umn.edu/). Please search by strain name or genotype. The neural activity data from this project, together with analysis code, plots of activity traces, phase trajectories, and time trace correlations for all conditions, are available at this Zenodo repository (https://doi.org/10.5281/zenodo.7563053). The code is also available at this GitHub repository (https://github.com/samuellab/celegans-sensory-code).

Submitted 26 July 2022
Accepted 1 February 2023
Published 1 March 2023
10.1126/sciadv.ade1249

ScienceAdvances

Functional imaging and quantification of multineuronal olfactory responses in *C. elegans*

Albert Lin, Shanshan Qin, Helena Casademunt, Min Wu, Wesley Hung, Gregory Cain, Nicolas Z. Tan, Raymond Valenzuela, Leila Lesanpezeshki, Vivek Venkatachalam, Cengiz Pehlevan, Mei Zhen, and Aravinthan D.T. Samuel

Sci. Adv., **9** (9), eade1249.
DOI: 10.1126/sciadv.ade1249

Science Advances
AAAS

Supplementary Materials for

Functional imaging and quantification of multineuronal olfactory responses in *C. elegans*

Albert Lin *et al.*

Corresponding author: Albert Lin, albertlin@g.harvard.edu; Cengiz Pehlevan, cpehlevan@seas.harvard.edu; Mei Zhen, meizhen@lunenfeld.ca; Aravinthan D.T. Samuel, samuel@g.harvard.edu

Sci. Adv. **9**, eade1249 (2023)
DOI: 10.1126/sciadv.ade1249

This PDF file includes:

Supplement

Supplemental methods

A: Identifying neurons in the ZM10104 strain

The ZM10104 strain used in this experiment expresses two fluorescent proteins: GCaMP6s driven by the *ift-20* promoter, and wCherry driven by *gpc-1*. GCaMP6s expression was localized to neuronal nuclei to minimize spatial overlap of neighboring neurons, and to make identification of neurons easier. The promoter *ift-20* drives GCaMP expression in all ciliated sensory neurons. Our neurons of interest, the chemosensory neurons, lie in the lateral ganglia, but note that this promoter is pan-sensory, driving expression in cells outside of the lateral ganglia. The wCherry landmark is expressed in the cytoplasm of AFD, AWB, ASI, ASE, AWC, and ASJ. Note that it also is expressed in RIB, a neuron which is not labeled with GCaMP.

Relative positions are given in the orientation in **Figure S1**, with the nose to the left, the tail to the right, dorsal top, and ventral bottom. Relative positions should be interpreted as “usually but not always," unless otherwise noted. Also note that overly compressing an animal in any direction will distort the relative positions. Before identifying neurons, it is important to identify the orientation of the animal in the recording by figuring out where the dorsal-ventral (DV) plane lies. This is most easily done by identifying the plane of bilateral symmetry. Once you have oriented yourself, you can begin to identify neurons.

The easiest neurons to immediately identify in this strain are ASH, ASJ, and the anterior “triplet" of ASK, ADL, ASI. It is often effective to identify these neurons first, then work on the other neurons using the color landmarks and process of elimination. AWC and ASE should usually be in the neighborhood of ASH, and the four neurons AWA, AWB, ADF, and ASG are between ASH and the anterior triplet. These four neurons occasionally overlap. To avoid signal mixing, overlapping neurons were excluded from the dataset. For each odorant condition, neuronal identification was carried out independently by at least two individuals.

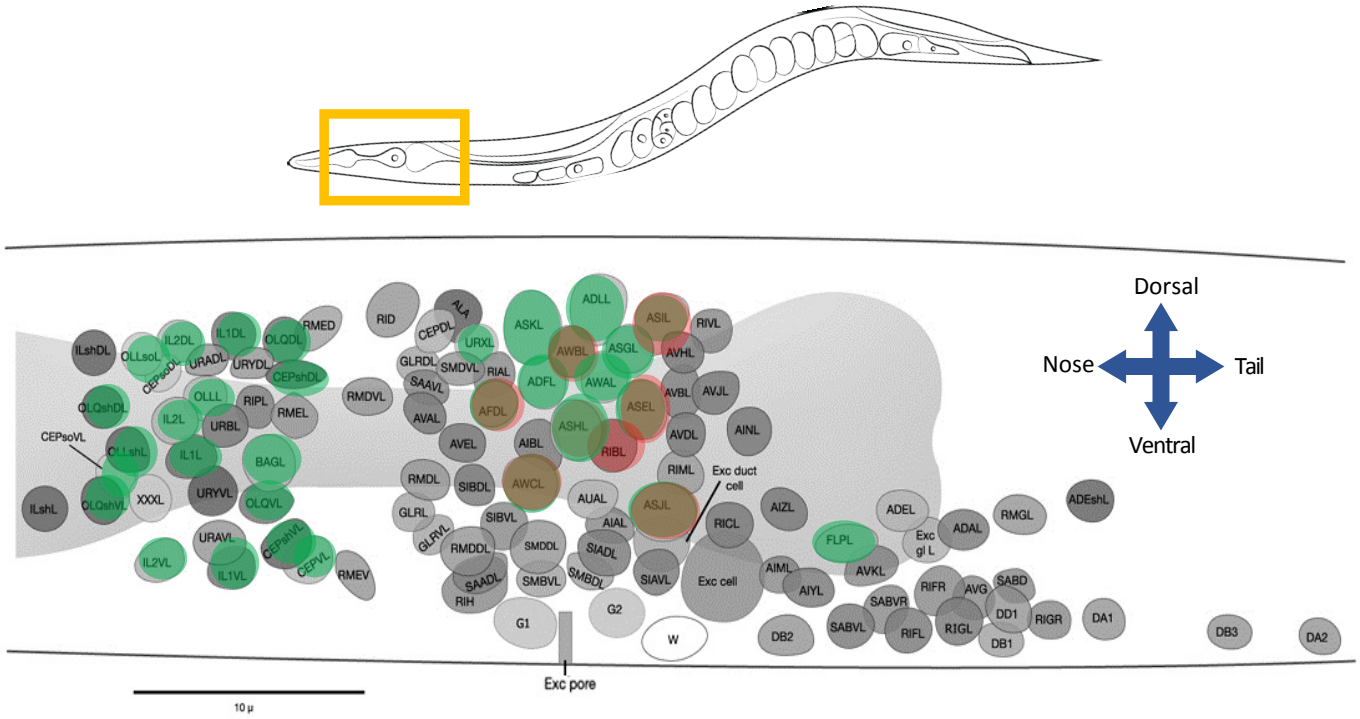

Figure S1. Identifying neurons in the ZM10104 strain. The *ift-20* promoter drives GCaMP expression in the nuclei of ciliated sensory neurons. The nuclei of the chemosensory neurons are all posterior to the nerve ring. A red landmark is provided by cytoplasmic expression of wCherry in the neurons AFD, AWB, ASI, ASE, AWC, and ASJ. Underlying *C. elegans* figure adapted from the digital version of White et al. 1986 (Wormbook)(50).

Table S1: Criteria for identifying each neuron class

Neuron	Color(s)	Relative Position	Notes
ASK	green	leftmost of the anterior triplet	large. do not confuse with URX, a small oblong neuron above ASK
ADL	green	part of the anterior triplet	larger than ASI
ASI	green & red	part of the anterior triplet	use color to distinguish from ADL
ASH	green & red	left of ASE, below AWA	bright, circular
ASE	green & red	right of ASH	smaller than ASH
AWC	green & red	variable. below ASH but can be to the left, directly below, or to the right	often oblong in shape
ASJ	green & red	tail end of the ganglion, bottom left	distance from AWC can vary
AWA	green	variable. usually above ASH	smaller than ASH, circular
AWB	green & red	position variable, usually directly below the anterior triplet	small, dim, a bit oblong. use color to identify
ADF	green	usually left of AWA, AWB	dim
ASG	green	usually right of AWA, AWB	small, circular

To minimize the chances of incorrect identification, neuronal IDs for each odorant condition were reviewed by at least two individuals, and ambiguous neurons were omitted from the analyzed datasets.

B: Olfactory stimuli and behavioral valences

Table S2: List of odorants

Odorant	Chemical class	Behavioral valence (low conc.)
1-pentanol	alcohol	attractive
1-hexanol	alcohol	attractive
1-heptanol	alcohol	repulsive
1-octanol	alcohol	repulsive
1-nonanol	alcohol	repulsive
isoamyl alcohol	alcohol	attractive
geraniol	alcohol	attractive
benzaldehyde	aromatic	attractive
methyl salicylate	aromatic	attractive
ethyl acetate	ester	attractive
ethyl butyrate	ester	attractive
ethyl heptanoate	ester	attractive
pentyl acetate	ester	attractive
butyl butyrate	ester	attractive
diacetyl	ketone	attractive
2-butanone	ketone	attractive
2-heptanone	ketone	attractive
2-nonanone	ketone	repulsive
2,3-pentanedione	ketone	attractive
2,5-dimethylpyrazine	pyrazine	attractive
2-methylpyrazine	pyrazine	attractive
2-isobutylthiazole	thiazole	attractive
2,4,5-trimethylthiazole	thiazole	attractive

C: Neuron tracking and signal extraction

To segment the neuronal nuclei in each recording, we built a GUI which allows users to navigate each 3D landmark image and click to add or remove neuron centers (21, 74). This GUI allows the user to toggle between multiple fluorescent channels and a maximum projection, allowing the user to take advantage of any fluorescent landmark labels in the strain. Complete labeling of all neuron centers is only necessary once for a given animal, even if multiple recordings have been made. The user then labels a small handful of widely spaced neurons (4-8) in the first frame of the activity recording. This small number of labeled neurons helps the tracking algorithm to compensate for any global motion or distortion that may have occurred in the animal between the landmark volume and the activity movie. In addition to segmentation, the GUI allows neurons to be manually identified. The names the user applies are then associated with the activity traces of those neurons.

Neighborhood correlation tracking of individual neurons

While the entire brain of the worm can distort substantially across large distances, the neighborhood immediately surrounding a neuronal nucleus of interest tends to remain consistent, with little local deformation. Our image registration strategy relies on this fact. Instead of attempting to identify neuron centers in every frame, we try to match the neighborhood surrounding the neuron center in the first frame to the most similar neighborhood in the following frame. We then return the center of the new neighborhood as the position of the neuron center in the next frame.

We first employ this approach to map the neuron centers identified in the high-resolution landmark volume during the segmentation step onto the first frame of the activity movie, which is captured at a lower resolution. We then proceed to compare each frame of the movie to the next. The neighborhood correlation comparison is made independently for each neuron. While we lose some information about local deformations by not integrating information about how neighboring neurons are moving, we gain the ability to run the tracking of each neuron in a dataset as a parallel process, dramatically decreasing runtime. This also prevents a mistake in tracking one neuron from propagating to other nearby neurons. We run the tracking on a down-sampled version of the activity movie, also to improve runtime.

For a given neuron center, the tracking algorithm goes through the following steps:

1. Given the position of the given neuron center in the current frame, $n_t = (x_t, y_t, z_t)$, we identify the neuron's local 3D neighborhood N_t in that frame, the volume with dimensions $2a * 2b * 2c$, in the region spanned by $[x_t - a, x_t + a]$, $[y_t - b, y_t + b]$, and $[z_t - c, z_t + c]$.

2. We identify the naive center in frame $t+1$, from where we begin our search for the neighborhood most similar to N_t. For the first frame of the movie, this point is adjusted by a distance-weighted average of the manually labeled neurons: $n'_{t+1} = (x_t + \Delta\Sigma w x^i, y_t + \Delta\Sigma w y^i, z_t + \Delta\Sigma w z^i)$. For any other frame, we simply take the naive center as the center of the previous frame, $n'_{t+1} = n_t = (x_t, y_t, z_t)$.

3. Starting from the naive center n'_{t+1}, we perform image registration between the maximum intensity projections in x, y, and z of putative neighborhood N'_{t+1} and the previous neighborhood N_t, computing the pairwise correlation of these images. We then repeat this process, moving the putative center n'_{t+1} by 1 pixel per iteration until one of the following occurs:

   (a) The algorithm finds a putative neighborhood N'_{t+1} whose correlation with N_t exceeds the confidence threshold C (usually set at above 90%). This putative neighborhood is then defined as N_{t+1}.

   (b) The algorithm tests all putative neighborhoods within a maximum search radius $r_{\max}$ of the naive center n'_{t+1}, but failed to find a putative neighborhood whose correlation exceeds the confidence threshold C. The algorithm then returns the putative neighborhood with the highest correlation with N_t as N_{t+1}.

   (c) If no neighborhood is found with a correlation exceeding a minimum value, the neuron is considered lost in frame $t+1$, likely either due to motion taking the neuron outside the region of interest. No center is reported, and the last reported neighborhood N_t is used as the basis of comparison for following frames ($t+2, t+3$, etc.).

4. The center of neighborhood N_{t+1} is defined as the neuron center in this frame, n_{t+1}.

5. Repeat until the end of the activity movie is reached.

We can optimize the tracking parameters such as neighborhood size (a, b, c), maximum search radius $r_{\max}$, and confidence threshold C for both accuracy and speed for different imaging conditions.

Extracting calcium dynamics

To extract calcium signals, we first map the positions of each tracked neuron center back onto the original-resolution volumetric images. We then extract fluorescence values from these images. We identify a small volume around each neuron center, containing voxels whose fluorescence will be assigned to the neuron. This volume is set as 2 µm x 2 µm x 3 µm for our data. We compute the mean of the 10 brightest pixels within this volume to extract a raw fluorescence trace $F_r(t)$. We then account for photobleaching by exponential detrending, giving us a clean fluorescence activity trace $F(t)$. We then identify the background fluorescence F_0 for each neuron, and report normalized neuron activity $\Delta F/F_0$.

Manual proofreading of traces

Manual proofreading is an opportunity to improve data quality by removing neurons which have been mistracked, adjusting the computer-determined baseline fluorescence F_0, and correcting or adding nuclear IDs. Proofreading also enabled us to remove traces which were contaminated by signals from neighboring neurons. The software then compiles all processed traces for a given individual into a single data structure.

D: Imputing missing single-trial responses

Across trials of all neurons and all conditions, about 20% of the neuron responses were either not captured, or excluded due to tracking mistakes or signal contamination issues. To perform single-trial discrimination analysis in the (N-dimensional) neural response space, we first had to fill these missing data points in a reasonable and biologically motivated way.

For a given odorant and M trials, the peak responses of the $N = 11$ sensory neurons can be compiled in a matrix $R \in \mathbb{R}^{N \times M}$. Without any assumptions for the values R, it is impossible to infer the missing data. Fortunately, due to the intrinsic correlation between the responses of different olfactory neurons, the full response matrix R is low rank (as indicated by the PCA of neural responses). We can use this low-rank information to recover the missing entries: "matrix completion" algorithms can solve this problem very efficiently (77, 78).

To verify that matrix completion can indeed recover the missing entries faithfully, we performed a holdout evaluation. For the response matrix to each odor, we performed matrix completion after randomly removing 20 entries ($x_i, i = 1, \cdots, 20$). The imputed matrix is denoted as X^*. We then calculated the Pearson correlation coefficient ρ between the estimated entries x_i^* with the true entries x_i. The average value of ρ is around 0.7 (**Figure S6A-B**). We used the MATLAB code provided in (79) with default parameters for matrix completion (`https://github.com/udellgroup/Codes-of-FGSR-for-effecient-low-rank-matrix-recovery`). Specifically, we chose an algorithm based on minimization of the nuclear norm `MC_Nulcear_IALM`.

E: Computational methods for discriminability quantification

For binary classification of all odorant pairs, we used linear regression and a simple SVM (linear or Gaussian kernel). To decode odor identity from the entire single-trial dataset, we built a multi-class classifier. We concatenate all of the single-trial responses of the 23 odorants at high concentration. Each trial is an 11-dimensional point, one dimension for every neuron class. Each point has an associated label indicating the odorant identity. This data set was randomly divided into 10 parts, 9 of which are used as a training set (90%) and one which is used as a validation set (10%).

We used the MATLAB function `fitcecoc` to fit a multi-class model which supports both SVM and other classifiers. Mechanistically, this method reduces the problem of overall classification into a sequence of binary classification problems. The performance was quantified by the classification error, estimated using the `crossval` function. The confusion matrix was generated using the functions `kfoldPredict` and `confusionchart`. The training is repeated 10 times, using each of the 10 parts of the datasets as the validation set, and the results were compiled.

For the *in silico* knockouts, we removed neurons from the training dataset, resulting, for example in 10-dimensional responses when one neuron was removed. We trained the multi-class classifier as above.

F: Statistics, code, and software

All statistical computations and image analysis code were written and run in MATLAB using standard toolboxes, with the exception of the OME Bio-Formats API (used to read Nikon ND2 file formats) (80) and CET Perceptually Uniform Color Maps (81).

Supplemental figures

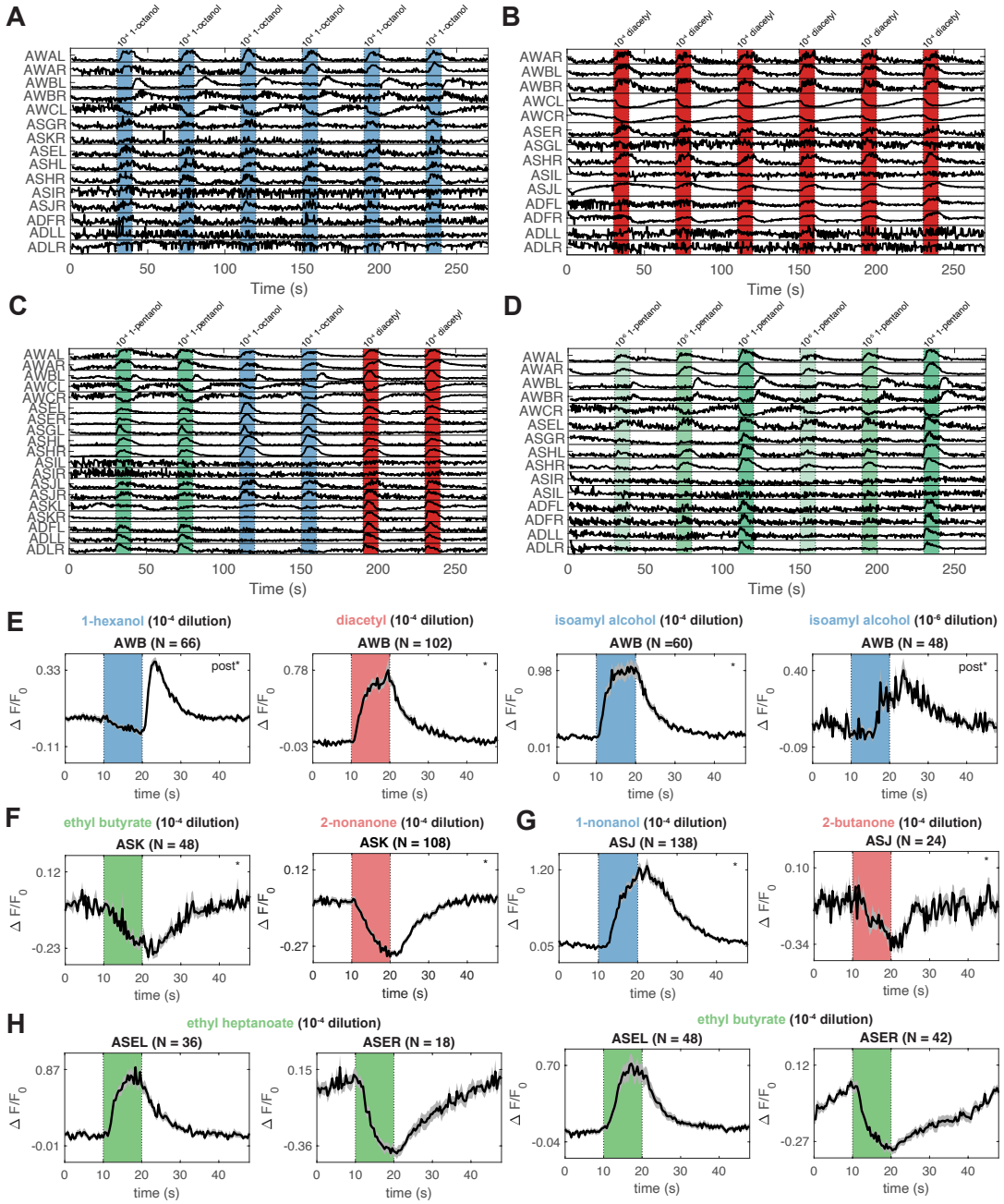

Figure S2. Single neuron response observations and example experiments. Examples of single experiments in which an animal was presented with multiple pulses of **(A)** 1-octanol and **(B)** diacetyl at the same concentration, demonstrating the consistency of sensory neuron responses under these conditions. Note that in each experiment, some neurons are missing due to occlusion or signal contamination. **(C)** A control experiment in which three odorants were presented to a single animal, evoking distinct and reproducible responses. **(D)** A control experiment in which one odorant (1-pentanol) was presented at 3 concentrations, evoking distinct and reproducible responses at each concentration. **(E)** AWB is an OFF response for most stimuli, such as 1-hexanol, but is occasionally an ON response, as is the case for high concentration diacetyl. High concentration isoamyl alcohol elicits an ON response from AWB, but low concentration isoamyl alcohol elicits an OFF response. This has been previously observed in Yoshida et al., 2012 (15). **(F)** We observe inhibitory responses to some odorants in ASK. **(G)** ASJ has an excitatory response to some odorants, such as 1-nonanol, but has an inhibitory response to 2-butanone. **(H)** We observe L/R asymmetries in ASE in response to several odorants, such as ethyl heptanoate and butyl butyrate.

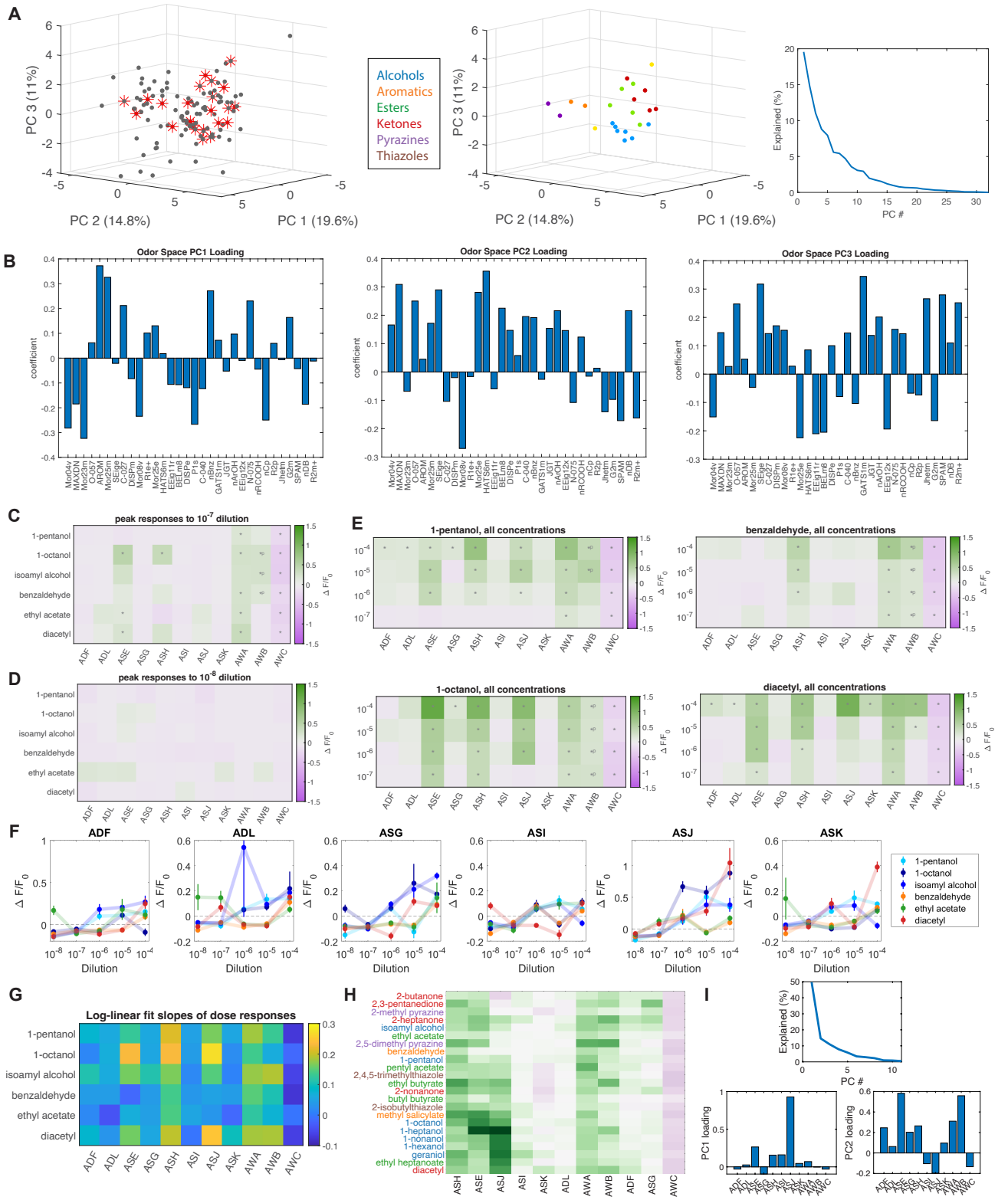

Figure S3. Supplemental panels for Figure 2. (A) An odor space constructed from the molecular descriptors of 122 odorants (gray) previously studied in *C. elegans*. We selected for our experiments a panel of 23 odorants (red) which span the odor space (left). These 23 odorants are presented in odor space colored by their chemical class (center). On the right is the variance explained as a function of the PC number in the odor space. **(B)** The molecular descriptor loadings of the first 3 principal components of the *C. elegans* odor space, plotted on the same axes. The leading components of PC 1 are measures of aromaticity, and the leading components of PC2 are measures of electronegativity. Peak responses for six odors tested at **(C)** 10^{-7} and **(D)** 10^{-8} dilutions. Statistically significant responses ($q \leq 0.01$) are indicated with stars—no significant activity was observed at the lowest tested dilution. **(E)** Compiled responses to three representative odorants at multiple concentrations (1-pentanol, 1-nonanol, and benzaldehyde) show similar neural responses across concentration. The magnitude of neuron responses generally increases with increasing concentration, and for some conditions, additional neurons are recruited at high concentration. **(F)** Dose responses for the six sensory neurons not printed in **Figure 2E**. **(G)** The fitted log-linear slopes m for the dose response of each neuron-odorant pair. The peak responses r as a function of odorant dilution c were fitted to the equation $r(c) \approx m \log_{10} c + I$, and the slope m was determined through linear regression. **(H)** Odorants (high concentration) clustered by their peak average neuronal responses. **(I)** The variance explained and the loadings of the first two principal components of the standardized average peak neural response PC space in **Figure 2F**.

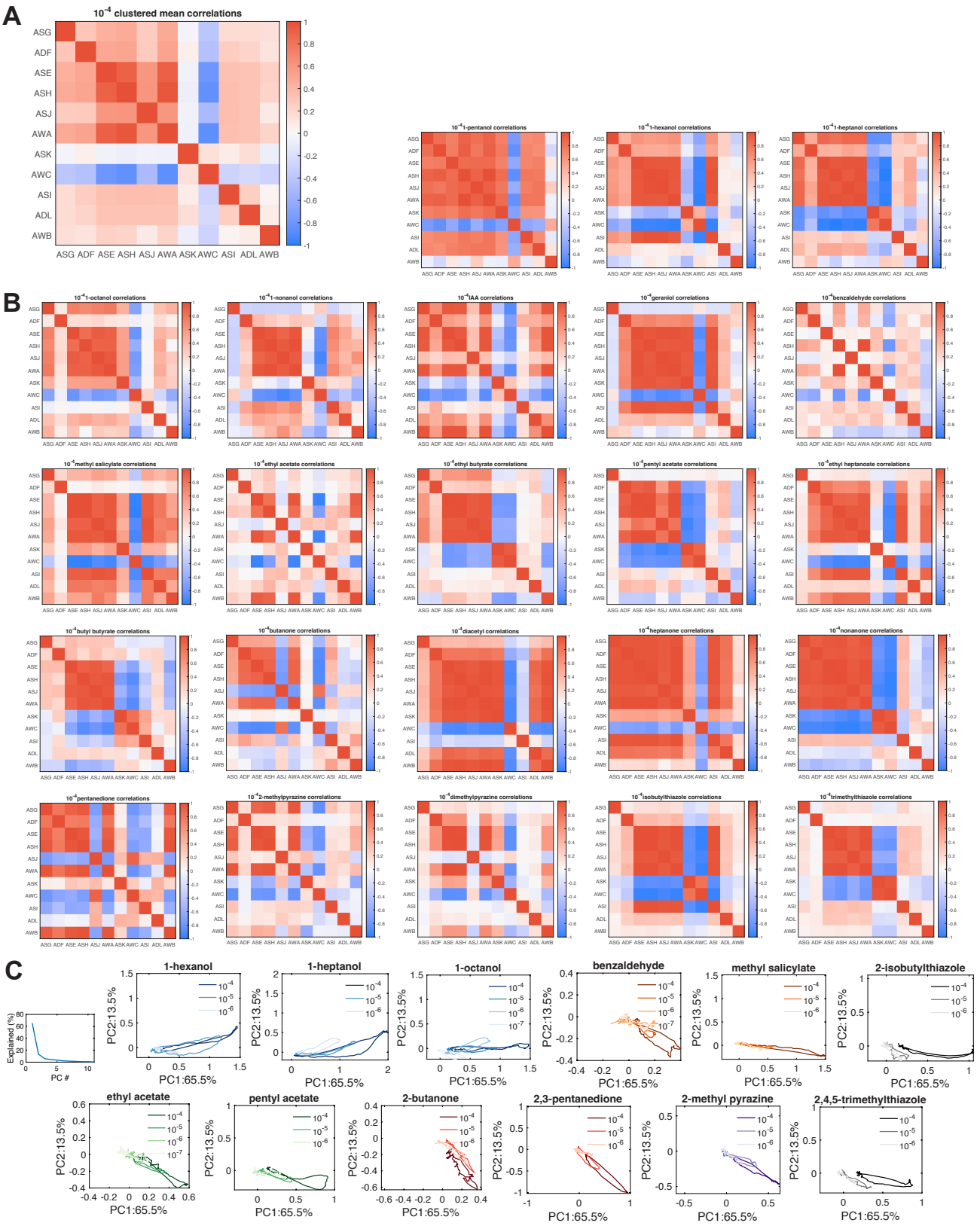

Figure S4. Time trace correlations and phase trajectory analyses. (A) Average time trace correlation map of the 11 chemosensory neuron responses across all 23 odorants. **(B)** Average correlation maps of responses to all 23 odorants at high concentration, plotted on the same axes, show diverse response dynamics. **(C)** Phase trajectory plots of average neural activity for select odorants, all plotted in a common PC space (Pareto plot of the PC space on the left). The shade of each color indicates concentration, with low concentration indicated by a light shade and high concentration indicated by a dark shade. Different concentrations of the same odorant tend to generate similar trajectories.

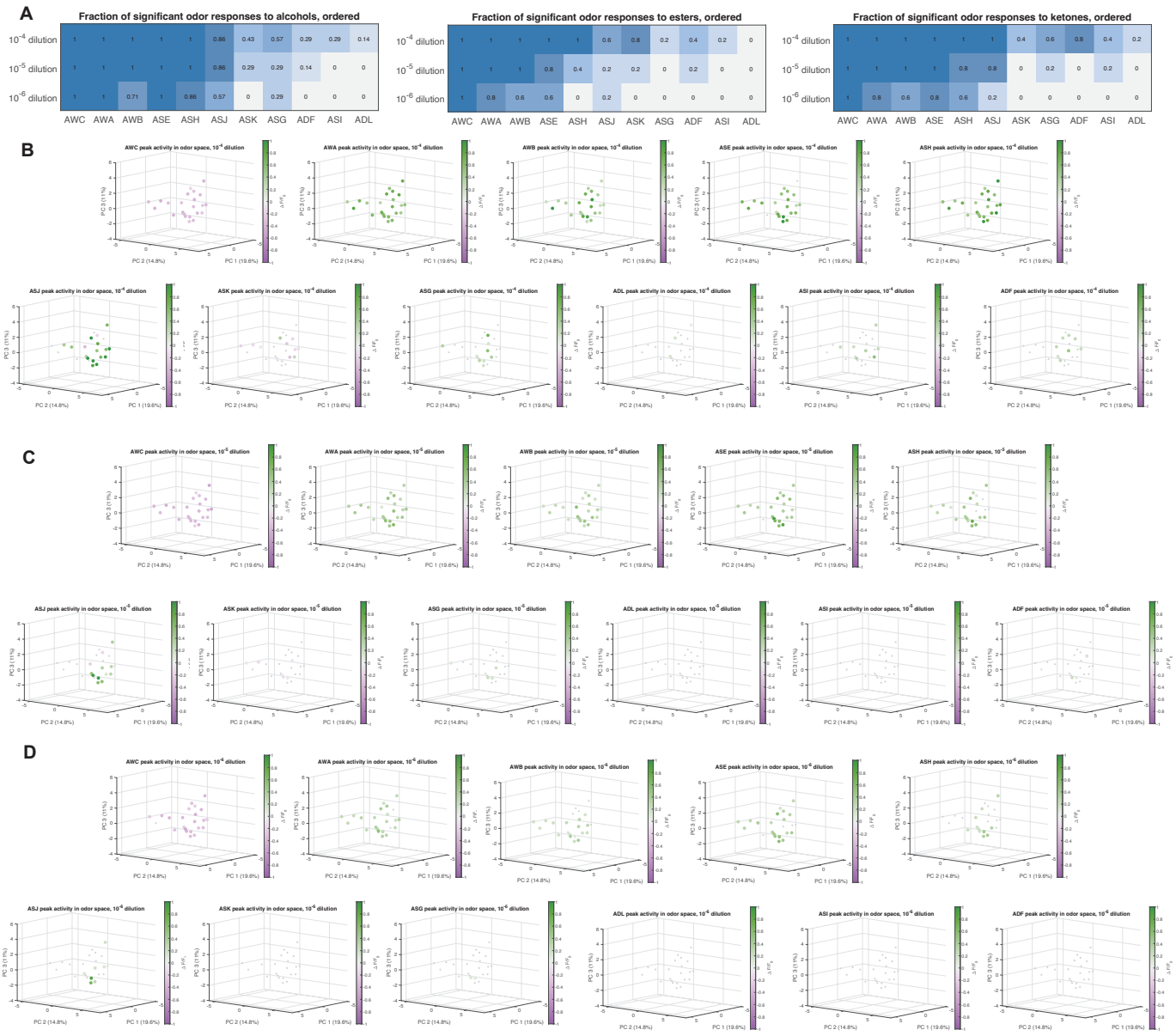

Figure S5. Average peak responses plotted in odor space. (A) The fraction of significant odor responses to three chemical groups: alcohols (7 total stimuli), esters (5 total stimuli), and ketones (5 total stimuli). Neurons are ordered by overall response fraction (**Figure 4A**). Average peak responses of each of the 11 chemosensory neuron classes plotted in odor space (**Figure S3A**), at **(B)** high odorant concentration (10^{-4}), **(C)** medium odorant concentration (10^{-5}), and **(D)** low odorant concentration (10^{-6}).

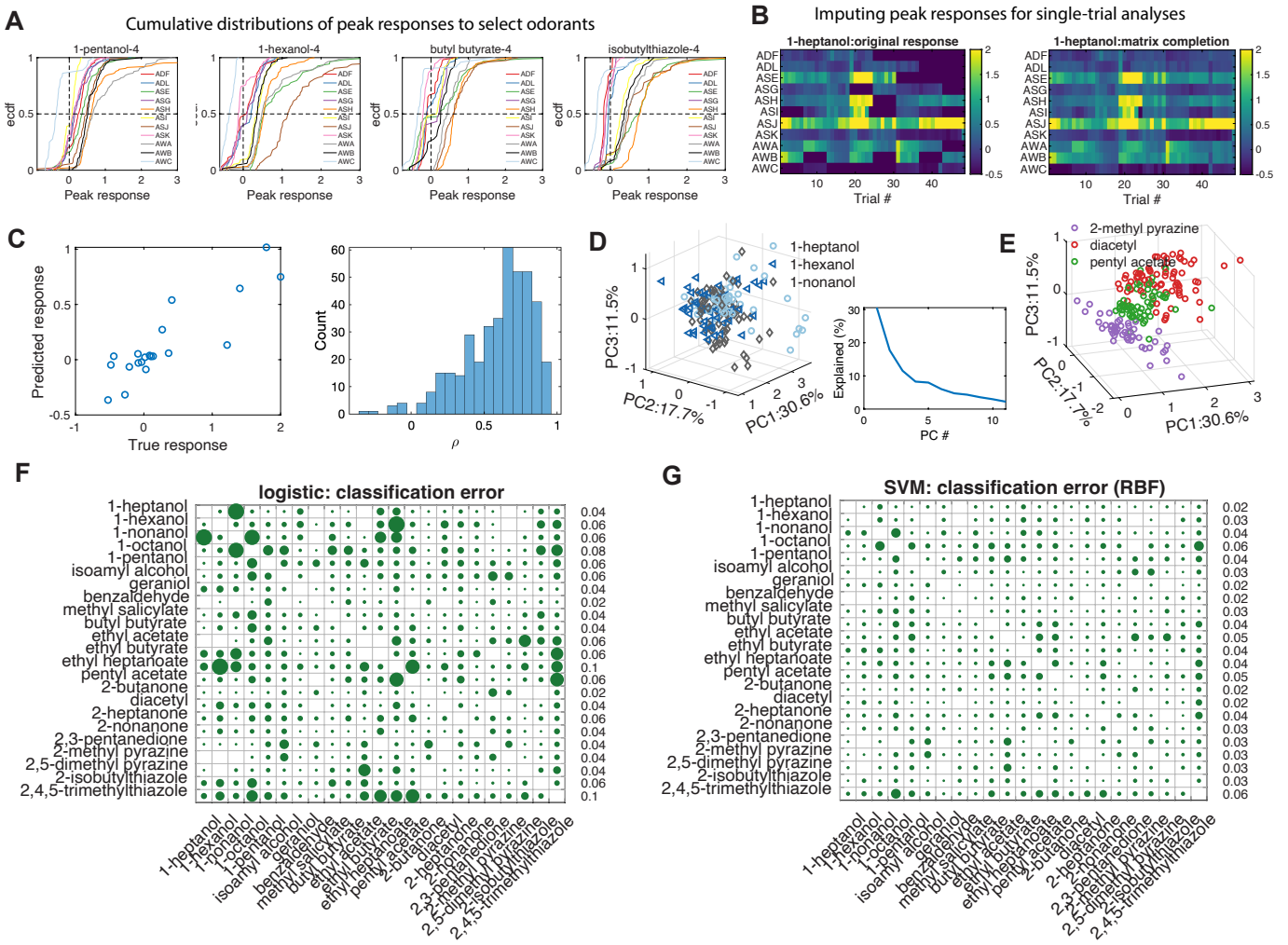

Figure S6. Supplemental panels for Figure 5. (A) Cumulative distributions of peak responses of every neuron (four exemplar odorants shown). **(B)** Signals were not always captured from all 22 chemosensory neurons in every trial. We used a matrix completion algorithm to impute these missing data points. Here are shown the peak responses all chemosensory neurons to 1-heptanol in different trials, with missing responses in dark blue (left) and after matrix completion (right). **(C)** *Left*: To quantify the performance matrix completion, we randomly removed 20 measured responses (true response) and compared the imputed values from matrix completion (predicted responses).*Right*: The histogram of Pearson's correlation coefficient between true responses and predicted responses. For each response matrix, we repeated 5 times. **(D/E)** Representations of single-trial peak neural responses to sets of **(D)** three similar and **(E)** three dissimilar odorants. These data are plotted in a PC space constructed from the individual trial responses to all odorants in the dataset. (Inset: The Pareto plot of the variance explained by each PC.) **(D)** We see that three similar odorants, the straight-chain alcohols 1-hexanol, 1-heptanol, and 1-nonanol, have more similar neural representations. **(E)** In contrast, three odorants of three distinct chemical classes, 2-methylpyrazine (a pyrazine), diacetyl (a ketone), and pentyl acetate (an ester), have more easily separable neural representations. Binary classification of all odorant pairs by **(F)** logistic regression and **(G)** SVM. Both methods return very low classification errors, demonstrating that the single-trial peak responses of any two odorants can be distinguished. Shown here are classification error heatmaps at high concentration (10^{-4} dilution), for which the average classification error is 0.055 for the logistic regression and 0.035 for the SVM.

REFERENCES AND NOTES

1. B. Malnic, J. Hirono, T. Sato, L. B. Buck, Combinatorial receptor codes for odors. *Cell* **96**, 713–723 (1999).

2. K. Nara, L. R. Saraiva, X. Ye, L. B. Buck, A large-scale analysis of odor coding in the olfactory epithelium. *J. Neurosci.* **31**, 9179–9191 (2011).

3. S. A. Kreher, D. Mathew, J. Kim, J. R. Carlson, Translation of sensory input into behavioral output via an olfactory system. *Neuron* **59**, 110–124 (2008).

4. G. Si, Jessleen K. Kanwal, Y. Hu, C. J. Tabone, J. Baron, M. Berck, G. Vignoud, A. D. T. Samuel, Structured odorant response patterns across a complete olfactory receptor neuron population. *Neuron* **101**, 950–962.e7 (2019).

5. J. W. Wang, A. M. Wong, J. Flores, L. B. Vosshall, R. Axel, Two-photon calcium imaging reveals an odor-evoked map of activity in the fly brain. *Cell* **112**, 271–282 (2003).

6. E. A. Hallem, J. R. Carlson, Coding of odors by a receptor repertoire. *Cell* **125**, 143–160 (2006).

7. J. del Marmol, M. A. Yedlin, V. Ruta, The structural basis of odorant recognition in insect olfactory receptors. *Nature* **597**, 126–131 2021.

8. M. De Bruyne, T. C. Baker, Odor detection in insects: Volatile codes. *J. Chem. Ecol.* **34**, 882–897 (2008).

9. P. S. Grewal, D. J. Wright, Migration of *Caenorhabditis elegans* larvae towards bacteria and the nature of the bacterial stimulus. *Fundam. Appl. Nematol.* **15**, 159–166 (1992).

10. C. I. Bargmann, H. Robert Horvitz, Chemosensory neurons with overlapping functions direct chemotaxis to multiple chemicals in *C. elegans*. *Neuron* **7**, 729–742 (1991).

11. C. I. Bargmann, Comparative chemosensation from receptors to ecology. *Nature* **444**, 295–301 (2006).

12. C. I. Bargmann, Chemosensation in *C. elegans*, *WormBook: The Online Review of C. elegans Biology* (2006), pp. 1–29; 10.1895/wormbook.1.123.1.

13. B. Vidal, U. Aghayeva, H. Sun, C. Wang, L. Glenwinkel, E. A. Bayer, O. Hobert, An atlas of *Caenorhabditis elegans* chemoreceptor expression. *PLOS Biol.* **16**, 1–34 (2018).

14. L. A. Perkins, E. M. Hedgecock, J. N. Thomson, J. G. Culotti, Mutant sensory cilia in the nematode *Caenorhabditis elegans*. *Dev. Biol.* **117**, 456–487 (1986).

15. K. Yoshida, T. Hirotsu, T. Tagawa, S. Oda, T. Wakabayashi, Y. Iino, T. Ishihara, Odour concentration-dependent olfactory preference change in *C. elegans*. *Nat. Commun.* **3**, 739 (2012).

16. J. Larsch, D. Ventimiglia, C. I. Bargmann, D. R. Albrecht, High-throughput imaging of neuronal activity in *Caenorhabditis elegans*. *Proc. Natl. Acad. Sci. U.S.A.* **110**, E4266–E4273 (2013).

17. S. G. Leinwand, C. J. Yang, D. Bazopoulou, N. Chronis, J. Srinivasan, S. H. Chalasani, Circuit mechanisms encoding odors and driving aging-associated behavioral declines in *Caenorhabditis elegans*. *eLife* **4**, e10181 (2015).

18. A. Zaslaver, I. Liani, O. Shtangel, S. Ginzburg, L. Yee, P. W. Sternberg, Hierarchical sparse coding in the sensory system of *Caenorhabditis elegans*. *Proc. Natl. Acad. Sci. U.S.A.* **112**, 1185–1189 (2015).

19. S. Yu, L. Avery, E. Baude, D. L. Garbers, Guanylyl cyclase expression in specific sensory neurons: A new family of chemosensory receptors. *Proc. Natl. Acad. Sci. U. S. A.* **94**, 3384–3387, (1997).

20. P. D. Wes, C. I. Bargmann, *C. elegans* odour discrimination requires asymmetric diversity in olfactory neurons. *Nature* **410**, 698–701 (2001).

21. E. Yemini, A. Lin, A. Nejatbakhsh, E. Varol, R. Sun, G. E. Mena, A. D. T. Samuel, L. Paninski, V. Venkatachalam, O. Hobert, NeuroPAL: A multicolor atlas for whole-brain neuronal identification in *C. elegans*. *Cell* **184**, 272–288–288.e11 (2021).

22. T. R. Thiele, S. Faumont, S. R. Lockery, The neural network for chemotaxis to tastants in *Caenorhabditis elegans* is specialized for temporal differentiation. *J. Neurosci.* **23**, 11904–11911 (2005).

23. H. Suzuki, T. R. Thiele, S. Faumont, M. Ezcurra, S. R. Lockery, and W. R. Schafer, Functional asymmetry in *Caenorhabditis elegans* taste neurons and its computational role in chemotaxis. *Nature* **454**, 114–117 (2008).

24. E. Z. MacOsko, N. Pokala, E. H. Feinberg, S. H. Chalasani, R. A. Butcher, J. Clardy, C. I. Bargmann, A hub-and-spoke circuit drives pheromone attraction and social behaviour in *C. elegans*. *Nature* **458**, 1171–1175 (2009).

25. A. Narayan, V. Venkatachalam, O. Durak, D. K. Reilly, N. Bose, F. C. Schroeder, A. D. T. Samuel, J. Srinivasan, P. W. Sternberg, Contrasting responses within a single neuron class enable sex-specific attraction in *Caenorhabditis elegans*. *Proc. Natl. Acad. Sci. U.S.A.* **113**, E1392–E1401 (2016).

26. J. S. Greene, M. Brown, M. Dobosiewicz, I. G. Ishida, E. Z. Macosko, X. Zhang, R. A. Butcher, D. J. Cline, P. T. McGrath, C. I. Bargmann, Balancing selection shapes density-dependent foraging behaviour. *Nature* **539**, 254–258 (2016).

27. E. Z. Aprison, I. Ruvinsky, Counteracting ascarosides act through distinct neurons to determine the sexual identity of *C. elegans* pheromones. *Curr. Biol.* 2589–2599.e3 **27**, (2017).

28. K. A. Fagan, J. Luo, R. C. Lagoy, F. C. Schroeder, D. R. Albrecht, D. S. Portman, A single-neuron chemosensory switch determines the valence of a sexually dimorphic sensory behavior. *Curr. Biol.* **28**, 902–914.e5 (2018).

29. P. T. McGrath, I. Ruvinsky, A primer on pheromone signaling in *Caenorhabditis elegans* for systems *biologists. Curr. Opin. Syst. Biol.* **13**, 23–30 (2019).

30. M. A. Hilliard, C. I. Bargmann, P. Bazzicalupo, *C. elegans* responds to chemical repellents by integrating sensory inputs from the head and the tail. *Curr. Biol.* **12**, 730–734 (2002).

31. M. A. Hilliard, C. Bergamasco, S. Arbucci, R. H. A. Plasterk, P. Bazzicalupo, Worms taste bitter: ASH neurons, QUI-1, GPA-3 and ODR-3 mediate quinine avoidance in *Caenorhabditis elegans*. *EMBO J.* **23**, 1101–1111 (2004).

32. J. M. Kaplan, H. R. Horvitz, A dual mechanosensory and chemosensory neuron in *Caenorhabditis elegans*. *Proc. Natl. Acad. Sci. U.S.A.* **90**, 2227–2231 (1993).

33. Y. Sambongi, T. Nagae, Y. Liu, T. Yoshimizu, K. Takeda, Y. Wada, M. Futai, Sensing of cadmium and copper ions by externally exposed ADL, ASE, and ASH neurons elicits avoidance response in *Caenorhabditis elegans*. *Neuroreport* **10**, 753–757 (1999).

34. A. Metaxakis, D. Petratou, N. Tavernarakis, Multimodal sensory processing in *Caenorhabditis elegans*. *Open Biol.* **8**, (2018).

35. C. I. Bargmann, E. Hartwieg, H. R. Horvitz, Odorant-selective genes and neurons mediate olfaction in *C. elegans*. *Neuron* **74**, 515–527 (1993).

36. S. H. Chalasani, N. Chronis, M. Tsunozaki, J. M. Gray, D. Ramot, M. B. Goodman, C. I. Bargmann, Erratum: Dissecting a circuit for olfactory behaviour in *Caenorhabditis elegans*. *Nature* **451**, 63–70 (2008).

37. M. Tsunozaki, S. H. Chalasani, C. I. Bargmann, A behavioral switch: cgmp and pkc signaling in olfactory neurons reverses odor preference in *C. elegans*. *Neuron* **59**, 959–971 (2008).

38. E. R. Troemel, B. E. Kimmel, C. I. Bargmann, Reprogramming chemotaxis responses: Sensory neurons define olfactory preferences in *C. elegans*. *Cell* **91**, 161–169 (1997).

39. Heon-ick Ha, M. Hendricks, Y. Shen, C. V. Gabel, C. Fang-Yen, Y. Qin, D. Colón-Ramos, K. Shen, A. D. T. Samuel, Y. Zhang, Functional organization of a neural network for aversive olfactory learning in *Caenorhabditis elegans*. *Neuron* **68**, 1173–1186 (2010).

40. D. Cheng, J. S. Lee, M. Brown, M. S. Ebert, P. T. McGrath, M. Tomioka, Y. Iino, C. I. Bargmann, Insulin/igf signaling regulates presynaptic glutamate release in aversive olfactory learning. *Cell Rep.* **41**, 111685 (2022).

41. M. Dobosiewicz, Q. Liu, C. I. Bargmann, Reliability of an interneuron response depends on an integrated sensory state. *eLife* **8**, e50566 (2019).

42. H. A. Colbert, C. I. Bargmann, Odorant-specific adaptation pathways generate olfactory plasticity in *C. elegans*. *Neuron* **14**, 803–812 (1995).

43. N. D. L'Etoile, C. M. Coburn, J. Eastham, A. Kistler, G. Gallegos, C. I. Bargmann, The cyclic GMP-dependent protein kinase EGL-4 regulates olfactory adaptation in *C. elegans*. *Neuron* **36**, 1079–1089 (2002).

44. G. Jansen, D. Weinkove, R. H. A. Plasterk, The G-protein γ subunit gpc-1 of the nematode *C. elegans* is involved in taste adaptation. *EMBO J.* **21**, 986–994 (2002).

45. M. A. Hilliard, A. J. Apicella, R. Kerr, H. Suzuki, P. Bazzicalupo, W. R. Schafer, In vivo imaging of *C. elegans* ASH neurons: Cellular response and adaptation to chemical repellents. *EMBO J.* **24**, 63–72 (2005).

46. S. Levy, C. I. Bargmann, An adaptive-threshold mechanism for odor sensation and animal navigation. *Neuron* **105**, 534–548.e13 (2020).

47. M. Khan, A. H. Hartmann, M. P. O'Donnell, M. Piccione, A. Pandey, P.-H. Chao, N. D. Dwyer, C. I. Bargmann, P. Sengupta, Context-dependent reversal of odorant preference is driven by inversion of the response in a single sensory neuron type. *PLOS Biol.* **20**, e3001677 (2022).

48. Q. Liu, P. B. Kidd, M. Dobosiewicz, C. I. Bargmann, *C. elegans* AWA olfactory neurons fire calcium-mediated all-or-none action potentials. *Cell* **175**, 57–70.e17 (2018).

49. I. G McLachlan, T. S. Kramer, M. Dua, E. M. Diloreto, U. Dag, J. Srinivasan, S. W. Flavell, Diverse states and stimuli tune olfactory receptor expression levels to modulate food-seeking behavior. bioRxiv 2022.04.27.489714 [**Preprint**]. 28 April 2022. https://doi.org/10.1101/2022.04.27.489714.

50. N. Chronis, M. Zimmer, C. I. Bargmann, Microfluidics for in vivo imaging of neuronal and behavioral activity in *Caenorhabditis elegans*. *Nat. Methods* **4**, 727–731 (2007).

51. S. E. Worthy, L. Haynes, M. Chambers, D. Bethune, E. Kan, K. Chung, R. Ota, C. J. Taylor, E. E. Glater, Identification of attractive odorants released by preferred bacterial food found in the natural habitats of *C. elegans*. *PLOS ONE* **13**, 1–14 (2018).

52. R. Haddad, R. Khan, Y. K. Takahashi, K. Mori, D. Harel, N. Sobel, A metric for odorant comparison. *Nat. Methods* **5**, 425–429 (2008).

53. P. Sengupta, J. H. Chou, C. I. Bargmann, odr-10 Encodes a seven transmembrane domain olfactory receptor required for responses to the odorant diacetyl. *Cell* **84**, 899–909 (1996).

54. P. J. Summers, R. M. Layne, A. C. Ortega, G. P. Harris, B. A. Bamber, R. W. Komuniecki, Multiple sensory inputs are extensively integrated to modulate nociception in *C. elegans*. *J. Neurosci.*, **35**, 10331–10342 (2015).

55. J. G. White, E. Southgate, J. N. Thomson, S. Brenner, The structure of the nervous system of the nematode *Caenorhabditis elegans*. *Philos. Trans. R. Soc. Lond. B Biol. Sci.* **314**, 1–340 (1986).

56. D. Witvliet, B. Mulcahy, J. K. Mitchell, Y. Meirovitch, D. R. Berger, Y. Wu, Y. Liu, W. X. Koh, R. Parvathala, D. Holmyard, R. L. Schalek, N. Shavit, A. D. Chisholm, J. W. Lichtman, A. D. T. Samuel, M. Zhen, Connectomes across development reveal principles of brain maturation. *Nature* **596**, 257–261 (2021).

57. J. E. Richmond, W. S. Davis, E. M. Jorgensen, UNC-13 is required for synaptic vesicle fusion in *C. elegans*. *Nat. Neurosci.* **2**, 959–964 (1999).

58. H. Sass, Sensory encoding of odor stimuli in *Periplaneta americana*. *J. Comp. Physiol. A Neuroethol. Sens. Neural Behav. Physiol.* **107**, 49–65 (1976).

59. M. Meister, T. Bonhoeffer, Tuning and topography in an odor map on the rat olfactory bulb. *J. Neurosci.* **21**, 1351–1360 (2001).

60. H. Saito, Q. Chi, H. Zhuang, H. Matsunami, J. D. Mainland, Odor coding by a mammalian receptor repertoire. *Sci. Signal.*, **2**, ra9 (2009).

61. D. Zwicker, A. Murugan, M. P. Brenner. Receptor arrays optimized for natural odor statistics. *Proc. Natl. Acad. Sci. U.S.A.* **113**, 5570–5575 (2016).

62. S. Qin, Q. Li, C. Tang, Y Tu, Optimal compressed sensing strategies for an array of nonlinear olfactory receptor neurons with and without spontaneous activity. *Proc. Natl. Acad. Sci. U.S.A.* **116**, 20286–20295 (2019).

63. K. Kajiya, K. Inaki, M. Tanaka, T. Haga, H. Kataoka, K. Touhara, Molecular bases of odor discrimination: Reconstitution of olfactory receptors that recognize overlapping sets of odorants. *J. Neurosci.*, **21**, 6018–6025 (2001).

64. H. Spors, M. Wachowiak, L. B. Cohen, R. W. Friedrich, Temporal dynamics and latency patterns of receptor neuron input to the olfactory bulb. *J. Neurosci.* **26**, 1247–1259 (2006).

65. T. Wakabayashi, I. Kitagawa, R. Shingai, Neurons regulating the duration of forward locomotion in *Caenorhabditis elegans*. *Neurosci. Res.*, **50**, 103–111 (2004)..

66. P. A. Garrity, M. B. Goodman, A. D. Samuel, P. Sengupta, Running hot and cold: Behavioral strategies, neural circuits, and the molecular machinery for thermotaxis in C. *elegans* and *Drosophila*. *Genes Dev.*, **24**, 2365–2382 (2010).

67. H. S. Kaplan, M. Zimmer, Brain-wide representations of ongoing behavior: A universal principle? *Curr. Opin. Neurobiol.* **64**, 60–69 (2020).

68. A. Lin, D. Witvliet, L. Hernandez-Nunez, S. W. Linderman, A. D. T. Samuel, V. Venkatachalam, Imaging whole-brain activity to understand behaviour *Nat. Rev. Phys.*, **4**, 292–305 (2022).

69. M. Meister. On the dimensionality of odor space. *eLife*, **4**, e07865 2015).

70. C. Bushdid, M. O. Magnasco, L. B. Vosshall, A. Keller, Humans can discriminate more than 1 trillion olfactory stimuli. *Science* **343**, 1370–1372 (2014).

71. C. D. Wilson, G. O. Serrano, A. A. Koulakov, D. Rinberg, A primacy code for odor identity. *Nat. Commun.* **8**, 1477 (2017).

72. D. R. Albrecht, C. I. Bargmann, High-content behavioral analysis of *Caenorhabditis elegans* in precise spatiotemporal chemical environments. *Nat. Methods* **8**, 599–605 (2011).

73. J. P. Nguyen, A. N. Linder, G. S. Plummer, J. W. Shaevitz, A. M. Leifer. Automatically tracking neurons in a moving and deforming brain. *PLOS Comput. Biol.*, **13**, e1005517 (2017).

74. V. Venkatachalam, N. Ji, X. Wang, C. Clark, J. K. Mitchell, M. Klein, C. J. Tabone, J. Florman, H. Ji, J. Greenwood, A. D. Chisholm, J. Srinivasan, M. Alkema, M. Zhen, A. D. T. Samuel, Pan-neuronal imaging in roaming *Caenorhabditis elegans*. *Proc. Natl. Acad. Sci. U.S.A.* **113**, E1082–E1088.

75. K. M. Hallinen, R. Dempsey, M. Scholz, X. Yu, A. Linder, F. Randi, A. K. Sharma, J. W. Shaevitz, A. M. Leifer. Decoding locomotion from population neural activity in moving *C. elegans*. *eLife*, **10**, e66135 (2021).

76. J. D Storey. A direct approach to false discovery rates. *J. R. Stat. Soc. B* **64**:479–498, 2002.

77. E. Candès, B. Recht. Exact matrix completion via convex optimization. *Commun. ACM*, **55**, 111–119, (2012).

78. L. T. Nguyen, J. Kim, B. Shim, Low-rank matrix completion: A contemporary survey. *IEEE Access* **7**, 94215–94237 (2019).

79. J. Fan, L. Ding, Y. Chen, M. Udell. Factor group-sparse regularization for efficient low-rank matrix recovery. *Adv. Neural Inf. Process. Syst.* **32** (2019).

80. M. Linkert, C. T. Rueden, C. Allan, J. M. Burel, W. Moore, A. Patterson, B. Loranger, J. Moore, C. Neves, D. M. Donald, A. Tarkowska, C. Sticco, E. Hill, M. Rossner, K. W. Eliceiri, J. R. Swedlow, Metadata matters: Access to image data in the real world. *J. Cell Biol.* **189**, 777–782 (2010).

81. P. Kovesi, Good colour maps: How to design them. arXiv:1509.03700 [cs.GR] (12 September 2015).